Asymmetric Dependence of Dark Count Rates on Magnetic Field in differently shaped Superconducting Nanowire Single-Photon Detectors based on Niobium Nitride

Master Thesis

Jessica Britschgi

Universität Zürich UZH

Mathematisch-naturwissenschaftliche Fakultät der Universität Zürich

Xiaofu Zhang

Prof. Dr. A. Schilling

Zürich

October 2017

Abstract

Although there already have been many studies on Superconducting Nanowire Single Photon Detectors (SNSPD), much is still to be investigated to further improve their applicability in detecting photons with high precision and to enhance their performance properties, such as the dark count rate. In order to lower the rate of such false counts without incident photons, their origins and dependencies need to be understood. In this thesis a model is evaluated, that describes the dark count rates' dependence on perpendicularly applied magnetic fields for meander-shaped SNSPDs, especially when the dependence does not show the expected symmetry in regard to the sign of the magnetic field. Measurements with three differently shaped SNSPDs have been performed. We found that while a magnetic field in one direction causes the dark count rates to increase, a magnetic field in the opposite direction is able to decrease it. This could be well explained by the model on trial.

Contents

1 Introduction

The demand for devices with the ability to detect single photons with high efficiency and high temporal resolution is shared by a variety of technical areas such as astronomy, space-to-ground communications, time-of-flight ranging and bioluminescence. Especially optical quantum information (QI) applications such as quantum key distribution (where quantum objects like photons play a key role) are expected to make great progress in the next decades. Therefor a lot of research is put in the improvement of single-photon detectors. The requirements concerning these devices include a better signal-to-noise ratio, high detection efficiency, adequate spectral range and the ability to resolve the number of photons reaching the detector simultaneously [1].

A promising type of single-photon detectors, featuring single-photon sensitivity from visible to mid-infrared wavelengths, low dark counts, short recovery times and excellent timing resolution, is based on photon-absorption by a thin superconducting strip. Such a device – named *superconducting nanowire single photon detector (SNSPD)* – is the centrepiece of my thesis.

The work I am going to present can be looked on as the continuation of the studies published by Engel *et al.* in 2012 [2]. They investigated the count rates of a meander-shaped SNSPD made of tantalum nitride and found a somewhat surprising asymmetric dependency of the dark count[1] rate on the applied magnetic field. The model they used to describe the dark count rate's dependence on magnetic fields was then adapted taking into account the suggested explanation for this asymmetry, which evolves around the inequality of the meander-shape's turns (see sec. 2.4).

The purposes of the experiments as part of this thesis are firstly, to ascertain, if the asymmetric dependence of the dark count rate on the magnetic field can be reproduced with other SNSPD-devices; and secondly, we evaluate Engel's [2] approach to explain this. The evaluation will be based on the dark count rate measurements of differently shaped SNSPDs made of niobium nitride (NbN). We vary the strength of an applied magnetic field, the bias current and the temperature to investigate their influences on the dark count rate.

After a brief introduction of some basics of superconductivity (sec. 2.1), the functional principle of an SNSPD will be explained (sec. 2.2). It will be followed by the description of the findings of previous research that lead to the development of [2]'s dark-count-rate-formula on trial. The experimental setup to measure the dark count rate dependencies of our SNSPDs will be described in section 3. Eventually, our findings will be presented in section 4.

---

[1] See section 2.3

2 Superconducting Nanowire Single Photon Detectors (SNSPDs)

2.1 Superconducting characteristics

To begin with, a few basics of superconductivity will be briefly presented without going into detail. The purpose is to introduce some of the recurring superconductor-related expressions used in the subsequent description of an SNSPD's functional principle and our devices' characteristics.

2.1.1 Cooper pairs

An electric conduction with no resistance can exist in certain materials due to the pairing of a number of electrons into *Cooper pairs*, named after Leon Neil Cooper who first described this phenomenon in 1956 [3]. The Cooper pairs interact with the ion-lattice (phonons) of the material in a way that lets them flow through it without resistance.

2.1.2 Coherence length

In 1950, V. L. Ginzburg and L. D. Landau have published a successful theory to describe superconductivity [4]. This so-called Ginzburg-Landau theory produced a relevant characteristic length of a superconductor, the superconducting *coherence length* ξ. There are many different formulations of how this length can be understood. The simplest one is that it is the distance between two electrons of a Cooper pair [5][6]. It is also described as the largest non-superconducting distance a Cooper pair can tunnel through and represents the smallest length over which the density of Cooper pairs can vary [6]. The coherence length ξ is a relevant quantity when it comes to superconducting single photon detectors, for example because some of the detector's characteristics will depend on the ratio of its dimensions to the coherence length.

2.1.3 Type-I and type-II superconductors

Superconductors are separated into two categories: type-I and type-II superconductors. Type-I superconductors show the *Meissner-Ochsenfeld* effect – the expulsion of magnetic fields – as long as the field is weak enough. The magnetic field penetrates the surface of a superconductor in this Meissner-state only to a depth of the order of the **penetration depth** λ.

When the field strength exceeds the material-dependent critical value H_c, the superconductivity is destroyed and the normally conductive state sets in.

Our detector material (NbN) is a type-II superconductor that doesn't go straight into the normal state when exposed to a lower critical field H_{c1} but only at a higher field H_{c2}. In between those critical fields the material is still superconducting but the magnetic field is not expelled completely anymore. Vortices of supercurrents appear in the material parallel to the surface. Within their cores, which have a size of the order of the superconducting coherence length ξ, the material is in its normal state and can be penetrated by the magnetic field. The magnetic flux Φ through such a vortex is quantized. It's as large

as the so-called superconducting magnetic flux quantum $\Phi_0 = \frac{h}{2e} \approx 2.07 \cdot 10^{-15}$ Wb [7][8], where h is the Planck constant and e is the electron charge.

The density of vortices in a superconductor increases the closer the magnetic field gets to the critical value H_{c2}.

Fig. 1 shows a sketch of vortices in a type-II superconductor, Fig. 2 two images of vortices in superconducting strips.
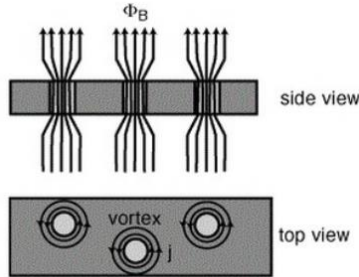

Fig. 1, [26]: Illustration of vortices in a type-II superconductor that is exposed to a magnetic field > H_{c1}.
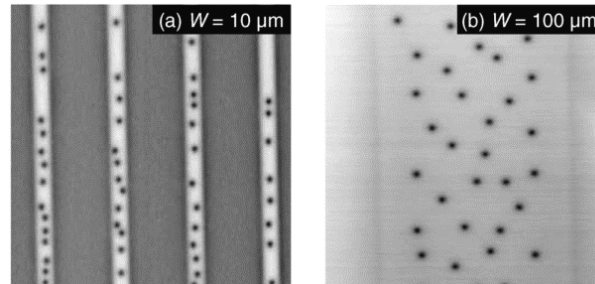
Fig. 2, [9]: Images taken of superconducting strips, where vortices are visible as dark spots and areas that expel the magnetic field appear white.

2.1.4 Pearl length or effective penetration depth

The *Pearl length* Λ describes the dimension of the magnetic field distribution around the core of a vortex of supercurrent in a thin type-II superconducting film. It is defined by $\Lambda = 2\lambda^2/d$, where λ is the London penetration depth and d is the thickness of the film. It is also called the *effective penetration depth*.

2.1.5 Transition from superconducting to normal state

The superconductive state of a material can be destroyed in various ways, but all of them result in supplying the electrons in the Cooper pairs with enough energy to break their bond. For example, this can be achieved by

a)   rising the temperature over a critical value,
b)   increasing the current density in a superconductor to a critical value, or
c)   exposing the superconductor to a strong enough magnetic field.

2.2 Functional principle of an SNSPD

As its name reveals, a superconducting nanowire single photon detector (SNSPD) is a device to detect single photons based on a superconducting strip with a width of the order of nanometres (a nanowire). The superconducting wire is fabricated onto an insulating substrate and is then integrated into a circuit. In order to be able to detect a photon, a bias current has to flow through the wire. How the absorption of a photon leads to a measurable signal is described by Bulaevskii *et al.* [10] "in a somewhat oversimplified picture presented in the literature" and illustrated in Fig. 3: When a photon is absorbed by the superconducting strip of the detector, it creates a hot spot that leads to the area becoming normally conductive. Consequently, the supercurrent in the strip will be forced to flow through the remaining superconducting area around the hot spot. There, the current density will be increased to a critical value, whereby this area is transformed to the normal state too. That way a normally conductive belt is created across the strip. Its resistance produces a measurable voltage pulse (Fig. 4), by what the incident photon is counted. Afterwards the normal belt will cool down again and the wire will return to its superconducting state, ready to detect another incident photon.
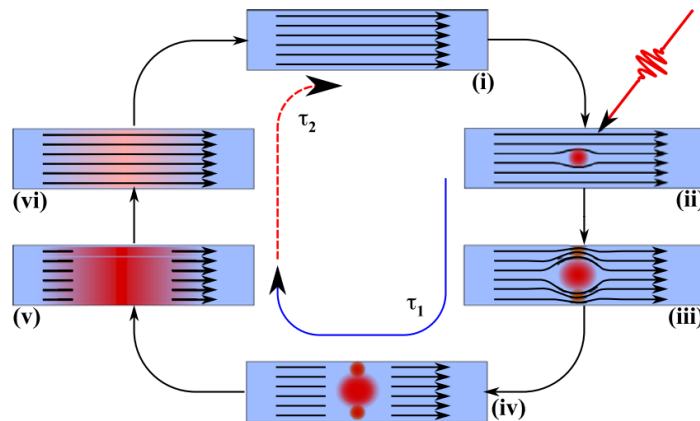

Fig. 3, [11]: Diagram of the detection principle of a SNSPD. (i) A bias current runs through the superconducting strip. (ii) The absorption of an incident photon leads to a hot spot. (iii) The current is forced to flow around the normally conducting hot spot, whereby the increased current density next to the hot spot causes the area to become normally conductive too. (iv) A belt-like region across the strip is transformed into the normal state → (v) A measurable voltage pulse is created due to the resistance of the normally conductive part of the strip. (vi) The heat dissipates in the material and the whole strip becomes superconducting again (i).
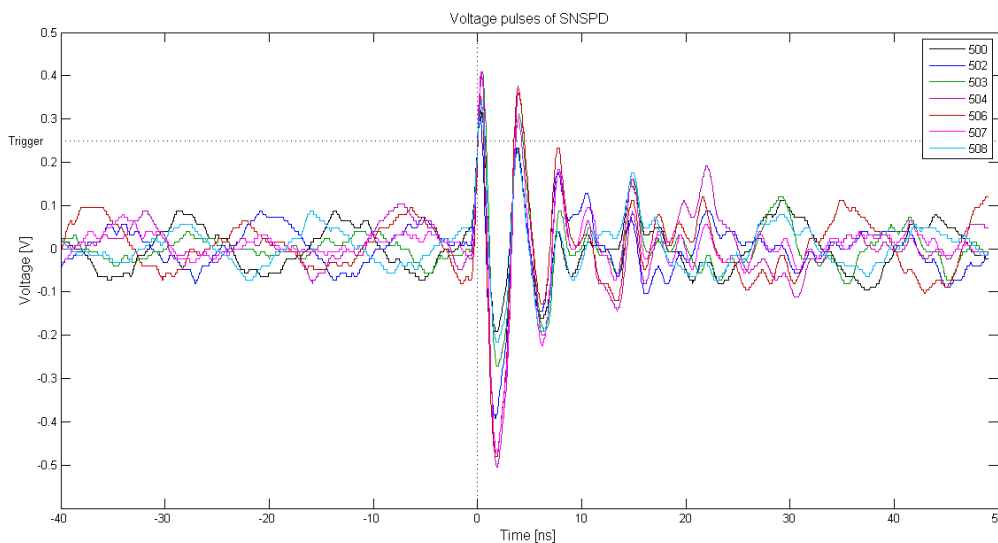

Fig. 4: Several voltage pulses of an SNSPD recorded by an oscilloscope.

2.2.1   Material choice: NbN

Superconductors are suitable to detect photons with wavelengths in the infrared, visible and even soft x-ray region [12] because of their energy gap – the energy required to excite electrons from the bound state (Cooper pairs) to the normal state - in the meV-range [13].

SNSPDs can be made out of various superconducting materials such as tantalum nitride (TaN), amorphous tungsten silicide (WSi), magnesium diboride (MgB$_2$) [14], niobium titanium nitride (NbTiN) [11] and the commonly used niobium nitrid (NbN). Other materials like molybdenum silicide (MoSi), molybdenum germanium (MoGe) and tungsten rhenium (WRe) are also in investigation for the use in SNSPDs [15].

The detectors examined in this thesis are made of NbN, as the first SNSPDs have been [11]. NbN-detectors are suitable to detect photons in the infrared and visible region. The feature making NbN the material of first choice is its very short thermalization time [16].

2.3   Dark Counts

In [17] Bulaevskii *et al.* wrote that three processes might cause voltage pulses that lead to counts in SNSPDs:

a) Enough Cooper pairs are broken apart by the energy of an absorbed photon to create a normal-state belt across the entire width of the strip (direct photon count),

b) A thermally induced single-vortex is formed and moves across the strip. If the bias current is high enough, the released energy by the vortex crossing is sufficient to transform a belt-like region across the strip width into the normal state. Hereby a so-called dark count is triggered, as there is no photon involved.

c) A "vortex-assisted single-photon count" happens by a combination of a) and b). When a single incident photon does not have enough energy to create a normal-state belt, it can still provoke a single-vortex crossing "which provides the rest of the energy needed to create the normal-state belt".

Within the scope of this thesis, the second process (dark count) is of most interest.

2.3.1   Vortex crossing

In a superconducting strip with thickness d on the order of the coherence length ξ and a larger width w much smaller than the Pearl length Λ, thus $d \approx \xi \ll w \ll \Lambda$, the main cause of dark counts is the formation of vortices that generate heat by crossing the strip orthogonally to the bias current due to the Lorentz force [10] (Fig. 5,6).

There exists an energy barrier for a vortex to enter a superconducting strip. It depends on the strip's bias current and the magnetic field it is exposed to.

For a strip width $w < 4.4\,\xi$ [18,19] it is possible for vortices to enter the strip solely because of the magnetic field generated by the bias current.
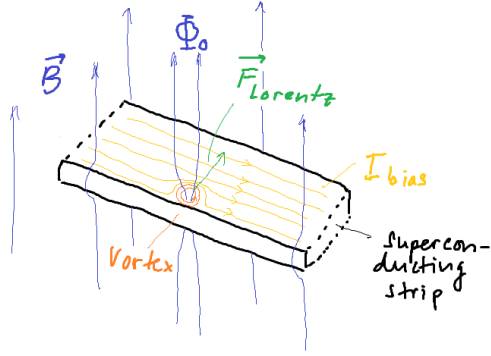
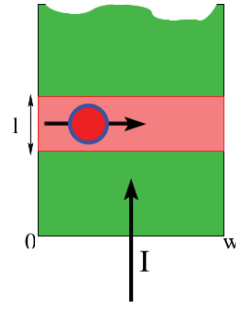Fig. 5: Sketch of a vortex in the superconducting strip of an SNSPD.

Fig. 6, [10]: Illustration of a vortex crossing a superconducting strip of an SNSPD, creating a hot belt.

2.3.2 Critical current

Clem *et al.* [20] showed that the highest current density in a strip with meander-shape is located in the sharp 180°-turns where current crowding takes place at the inner edge (Fig. 7). Consequently the critical current of such a structure is decreased as compared to that of only a straight strip, and the entry of vortices into the strip is most probable to happen in the 180°-turns. Engel *et al.* [2] estimated that the probability for vortex crossings are $\sim 10^5$ times higher near the turns as compared to the straight parts of the strips. Therefore, in order to describe the magnetic field depending dark count rate of our SNSPDs, we will focus on the contribution of the 180°-turns.
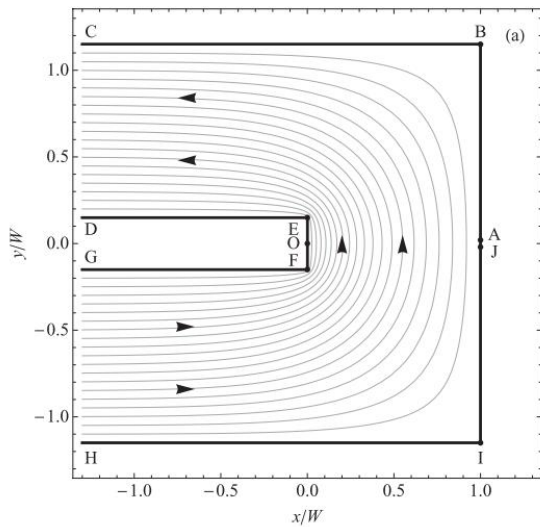

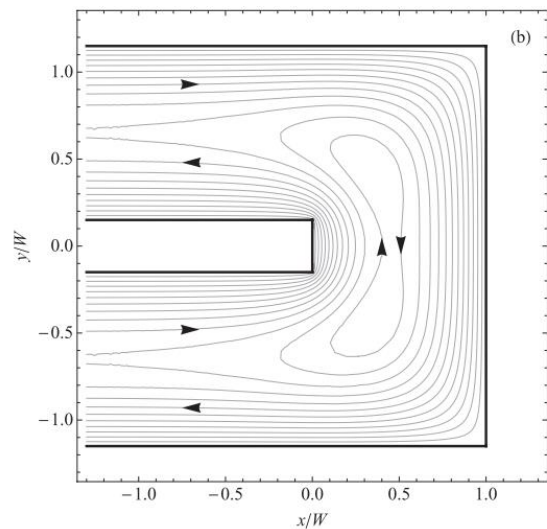Fig. 7, [21]: Current distribution in a rectangular 180°-turn. The current density is larger at the inner edges.

Fig. 8, [21]: Current distribution in a rectangular 180°-turn under the influence of a magnetic field perpendicular to the current.

2.3.3 Magnetic field dependence

In [17] it was shown that the vortex-crossing rate is enhanced by a magnetic field in combination with a bias current. At currents close to the critical current, the effect of the magnetic field is said to be equivalent to increasing the bias current by a factor $\left(1 + \frac{H}{H^*}\right)$, where H^* is a device-dependent field scale (see Eq. (2)).

10

The influence of a perpendicularly applied magnetic field on the current density in 180°-turns was examined by Clem et al. [21], Fig. 8. They found that screen currents in the strip caused by the magnetic field can increase or also decrease the current density near the inner edge of the turnaround, depending on the orientation of the field and the bias current (Fig. 10). If an applied magnetic field for example reduces the current density in a left turn of the strip, it will conversely enhance it in a right turn, as is sketched in Fig. 9.
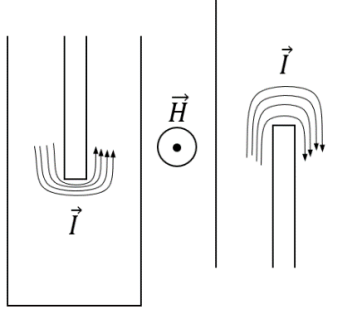

Fig. 9: Illustration of the current density being increased by a perpendicular magnetic field at one turn and decreased at a turn bent in the other direction.
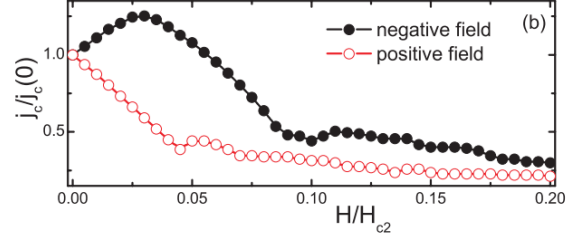

Fig. 10, [21]: Measurement results of a 180°-turn's critical current depending on a perpendicularly applied magnetic field.

According to [17] the field dependent critical current of a SNSPD like ours can be described by Eq. (1), if the magnetic field H is sufficiently smaller than H^*, which is the case in our experiments.

$$I_c(H) = I_{c0}\left(1 - \frac{H}{H^*}\right),$$ (1)

$$H^* \approx \frac{2w}{\pi e \xi} H_0, \quad H_0 = \frac{\Phi_0}{2\mu_0 w^2},$$ (2)

Here I_{c0} is the critical current in zero field and e is Euler's number; w is the strip width, ξ the coherence length, Φ_0 the magnetic flux quantum and μ_0 is the magnetic constant.

As was mentioned before, $I_c(H)$ will either be increased or decreased at the inner edge of a turn, depending on the current direction and the orientation of the magnetic field. In case of increasing the critical current, equation (1) should have a plus sign:

$$I_c(H) = I_{c0}\left(1 + \frac{H}{H^*}\right)$$ (3)

This can also be achieved by appointing a negative sign to the scale factor H^*.

2.3.4 Dark count rate

Engel et al. [2] agreed with Clem et al. [21] in that the field dependent critical current is the current for which the energy barrier for vortex entry vanishes, thus enabling a vortex to transition an area of the strip into the normal state by what a dark count is triggered. They described the dark count rate R_{DC}'s dependence on the current by

$$R_{DC} \approx R_0 \cdot \exp\left(\frac{I_b}{\tilde{I}}\right),$$ (4)

with R_0 being a proportionality factor and I_b the bias current in the strip. $\tilde{I}$ is a current scale proportional to the experimental critical current I_c, which we will express by γI_c, with γ being a dimensionless scale factor.

To describe the dark count rate generated at a single 180°-turn of the meander structure, Engel *et al.* [2] inserted Eq. (1) into Eq. (4). This yields

$$R_{DC}^1 \approx R_0 \cdot \exp\left(\frac{I_b}{\gamma I_{c0} \cdot \left(1 - \frac{H}{H^*}\right)}\right). \tag{5}$$

By this formula, the dark count rate of a turn would be increased by a positive magnetic field and decreased by a negative magnetic field.

If a positive magnetic field leads to an increased dark count rate in the meander-turns of one direction, it should decrease the dark count rate generated by the turns in the other direction.

To describe the dark count rate R_{DC}^M produced by a meander-shaped superconducting strip with a number of $N_\cup$ turns bent in one direction (e.g. left turns) and $N_\cap$ turns bent in the opposite direction (e.g. right turns), we summarize the contributions of the two types of turns as follows.

$$R_{DC}^M(H) = N_\cup \cdot R_{DC}^1(H) + N_\cap \cdot R_{DC}^1(-H) \tag{6}$$

If the meander consists of an equal number of left and right turns ($N_\cup = N_\cap$), the dark count rate R_{DC}^M should be symmetric regarding the sign of the magnetic field H. This was confirmed by the results of Lusche *et al.* [18][2]

2.4 Model for an asymmetric dependency of the dark count rate on the magnetic field

Engel *et al.* [2] studied the dependence of both the photon and dark count rate of a TaN-meander SNSPD on a magnetic field perpendicular to the meander plane. Although the detecting area consisted of a meander structure with an equal number of 180° turns in both directions, an asymmetry of the dark count rate as a function of magnetic field was found (Fig. 11). They suggested that this asymmetry could be caused by irregularities of the detector material, namely turns with impurities or small damages, where the current density would be increased. If the turns of one orientation were on the whole more flawed than the opposite turns, the effect of the magnetic field lowering the critical current and thus enhancing the rate of vortices crossing the strip would be greater there for the corresponding magnetic field direction. Instead of acknowledging several impurities in various turns, Engel proposed to summarize them all in one turn and to treat all the other turns as equal. For that purpose Eq. (6) was adapted to

$$R_{DC}^M(H) = (N_\cup - 1) \cdot R_{DC}^1(H) + R_{DC}^\beta(H) + N_\cap \cdot R_{DC}^1(-H), \tag{7}$$

where R_{DC}^β denotes the dark count rate generated in the "bad" turn. It can be expressed by

---

[2] They applied magnetic fields up to 100 mT though, what is ten times as strong as the applied magnetic fields in [2]. It is not visible in the plots how the dark count rates depend in detail on magnetic fields in the range $-10\,\text{mT} < B < 10\,\text{mT}$.

$$R_{DC}^{\beta} = R_0 \cdot \exp\left(\frac{I_b}{\beta \cdot \gamma I_c \left(1 - \frac{H}{H^*}\right)}\right), \tag{8}$$

with $0 < \beta < 1$ being the factor that implements the reduced critical current in that one turn. This model function (Eq. (7)) was suitable to describe the asymmetric dark count rate data [2] measured. We will evaluated how it fits our NbN-SNSPDs' dark count rate measurements.
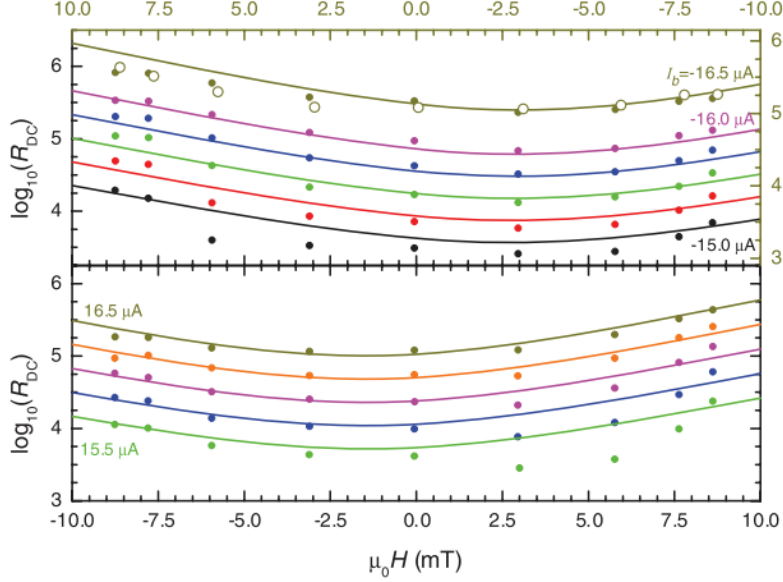

Fig. 11, [2]: Asymmetry of dark count rate vs. magnetic field measured with a TaN-SNSPD.

2.4.1 Dead time correction

The *dead time τ* of a detector is the duration of time after a detection during which the detector is not able to detect anew because it has not yet returned to its initial 'triggerable' state. If this dead time was longer than the time passing between two events theoretically causing dark counts, the measured dark count rate would be lower than the rate of those events. To take this into account the measured dark count rate can be modified as described by Willink [22]:

$$CR = \frac{CR_m}{1 - CR_m \cdot \tau} \tag{9}$$

Here CR is supposed to be the actual count rate and CR_m is the measured (observed) count rate. The dead time τ of our standard meander detector was estimated by using the outcome of a measurement with an interfering signal that is shown in Fig. 12. The shortest time interval between two successive triggers of the meander-detector was determined to be $\Delta t \approx 2.5$ µs, although the frequency of the signal reaching the threshold voltage was of the order of 70 GHz. To identify this time interval with the detector's dead time could be a mistake, as not every peak of the signal reaches the trigger threshold and other NbN-SNSPDs are reported to have dead times of the order of only 10 ns [1]. However, as the evaluation of our measured dark count rate data in section 4.3.2 shows, the dead-time correction with the value $\tau = 2.5$ µs seems not to be overestimated. In fact, none of our measurements yielded a dark count rate higher than $4 \cdot 10^5$ s^{-1}, what a least does not contradict the estimated dead time.

13
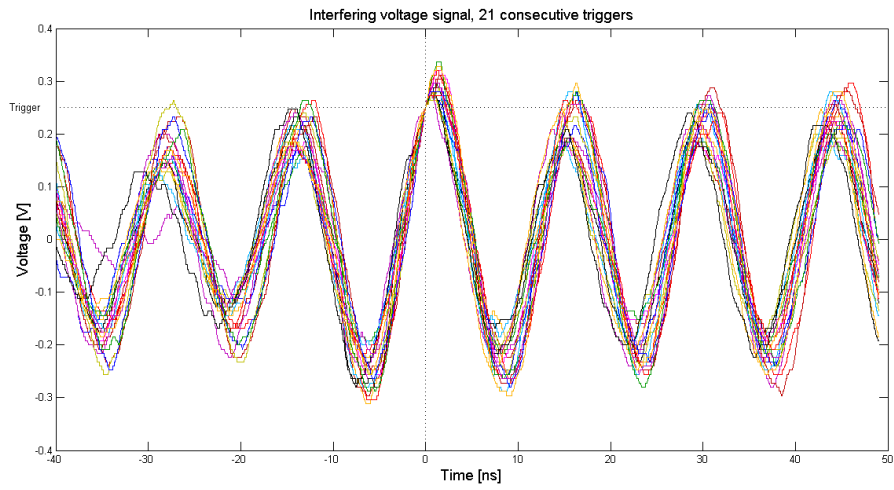
Fig. 12: Interfering signal (probably due to a faulty amplifier) triggering the oscilloscope recording; used to estimate the dead time of the SNSPD.

3 Experimental Setup

3.1 Devices

We want to investigate the dark count rates of three differently shaped SNSPDs made of niobium nitride (NbN). As we are assuming that sharp bends of a superconducting strip are the dominant region to generate dark counts, the three shapes differ in the number of turns. The first detector is standardly shaped like a meander with an equal number of left and right turns (Fig. 13). The second detector is meander-shaped too, but with a total of only five turns (Fig. 16). The third detector is no meander but a single bridge, therefor has no turns but only a straight strip (Fig. 19).

Characteristics of the three devices are listed in Table 1.

	2M	1M5	1B
	Meander detector with 28 turns and 30 straight strips	Meander detector with 5 turns and 6 straight strips	Single bridge detector with one straight strip
Thickness d [nm]	4	4	4
Width w [nm]	79.4	84.91	76.75
Total conductor length l [μm]	146.4	41.3	8
Critical temperature T_c [K]	13.155	13.262	12.715
Critical magnetic field $B_{c2}(0)$ (extrapol.) [T]	23.26	23.17	21.93
Coherence Length $\xi(0)$ [nm]	4.47	4.48	4.61
Effective penetration depth Λ [μm]	48.74	69.23	(unknown)

Table 1: Characteristics of the SNSPDs used in our experiments.

According to [13], the coherence length was derived from the critical magnetic flux density B_{c2} at zero temperature, which was determined by extrapolation of $B_{c2}(T)$-data provided by measurements with a PPMS®[3] device (Fig. 15, 18, 21).

$$\xi^2(0) = \sqrt{2} \cdot \frac{\phi_0}{2\pi \cdot B_{c2}(0)}. \tag{10}$$

---

[3] PPMS®: Physical Property Measurement System

Standard meander detector 2M

Fig. 13 a):
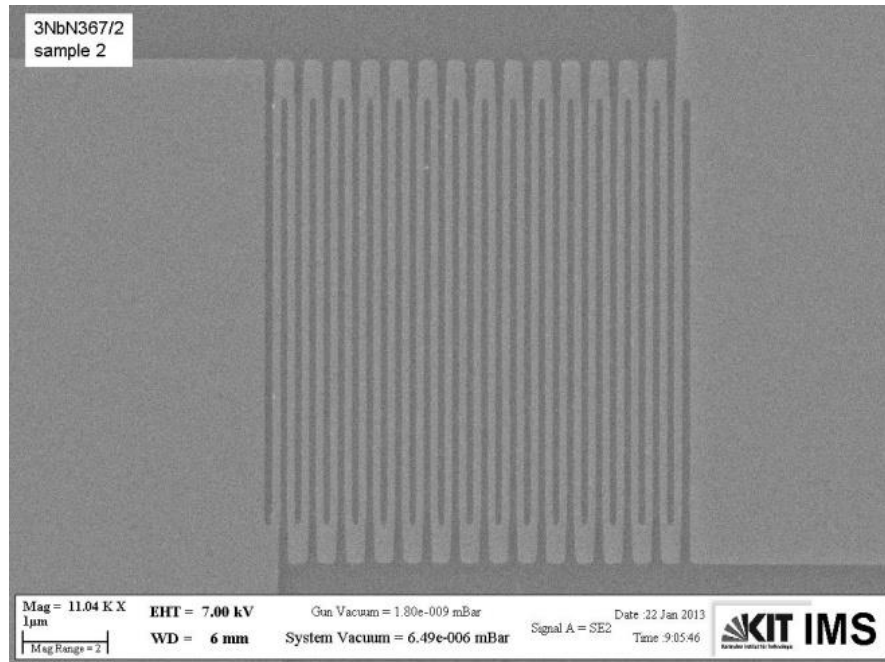Image of the standard meander SNSPD with 28 turns and 30 straight strips.

Fig. 13 b):
Close-up of the standard meander SNSPD. The strip width is 79.4 nm. Imperfections of the strip edges are visible.
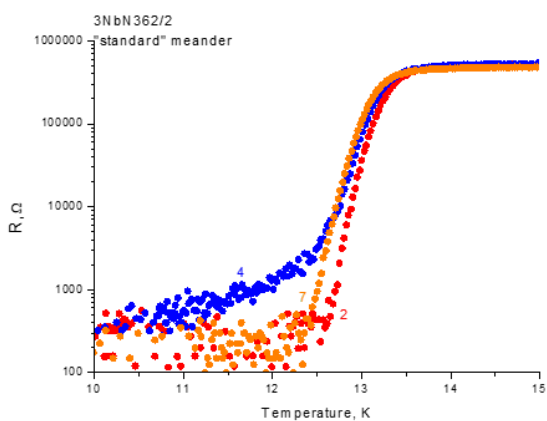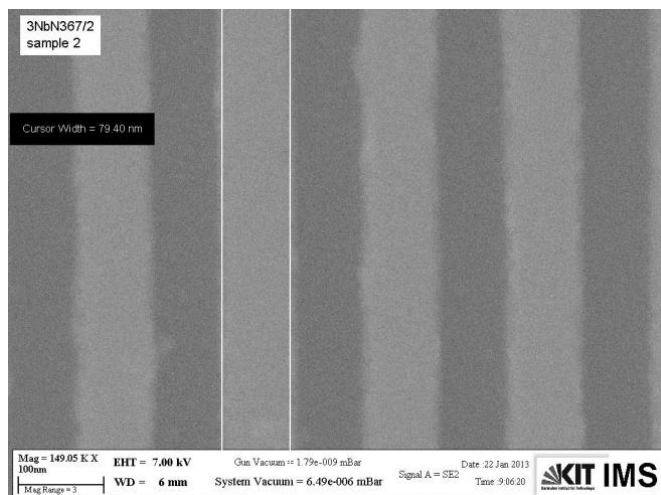

Fig. 14: Resistance vs. temperature of meander-SNSPDs, measured by Karlsruhe Institute of Technology. We chose to perform our experiments with sample 2.
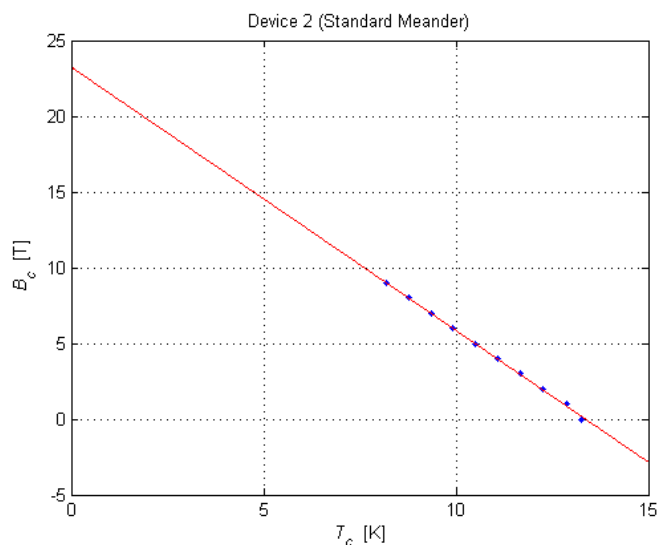

Fig. 15: Critical magnetic flux density vs. critical temperature, measured with a PPMS. The red line is a linear fit to extrapolate $B_c(0)$.
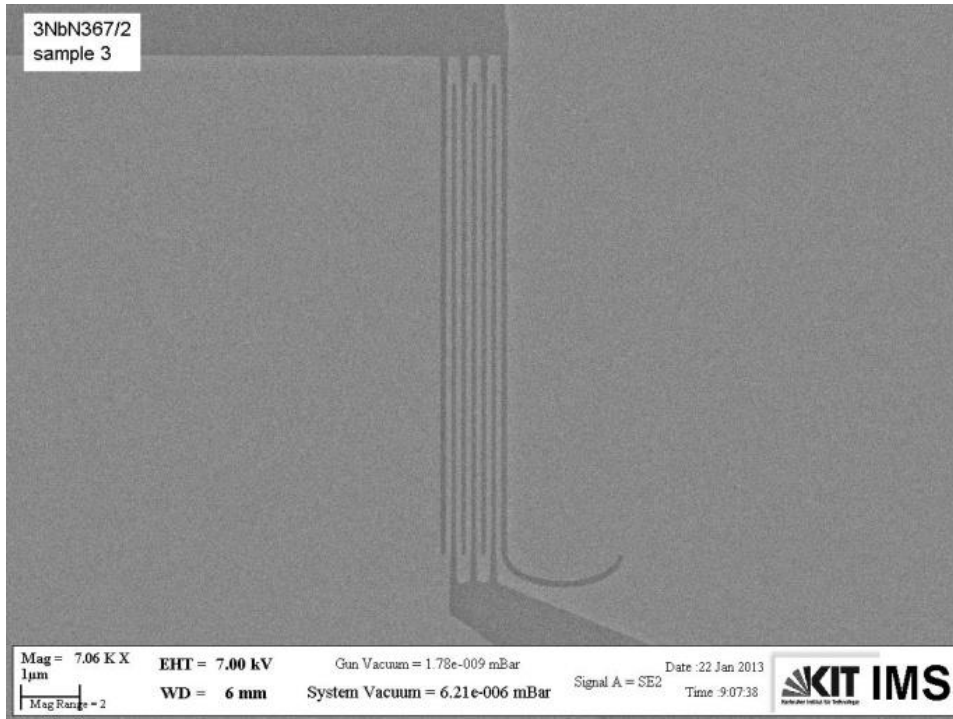
16

Five-turns meander detector 1M5

Fig. 16 a): Image of the five-turn meander SNSPD with five turns and six straight strips.
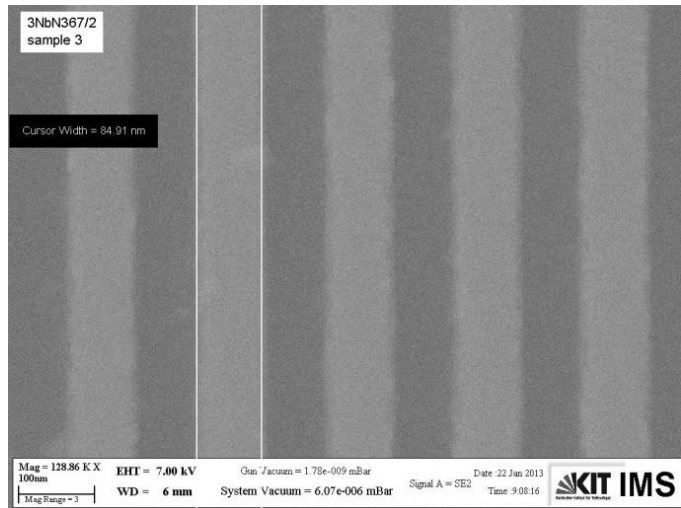

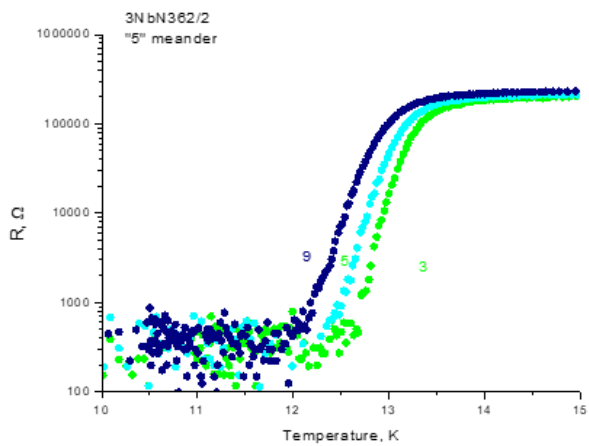**Fig. 16 b):** Close-up of the 5-turns meander SNSPD. The strip width is 84.91 nm.

Fig. 17: Resistance vs. temperature of 5-turns SNSPDs, measured by Karlsruhe Institute of Technology. We chose to perform our experiments with sample 3.
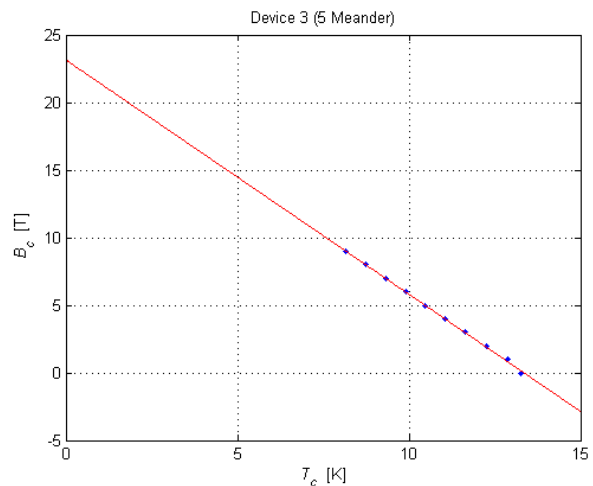

Fig. 18: Critical magnetic flux density vs. critical temperature, measured with a PPMS. The red line is a linear fit to extrapolate $B_c(0)$.

17

Single bridge detector 1B

Upper part of the single bridge detector. The current runs only through the middle strip.

Close-up of the single-bridge detector. The strip width is 76.75 nm.

Fig. 20: Resistance vs. temperature of single-bridge SNSPDs, measured by Karlsruhe Institute of Technology. We chose to perform our experiments with sample 1.
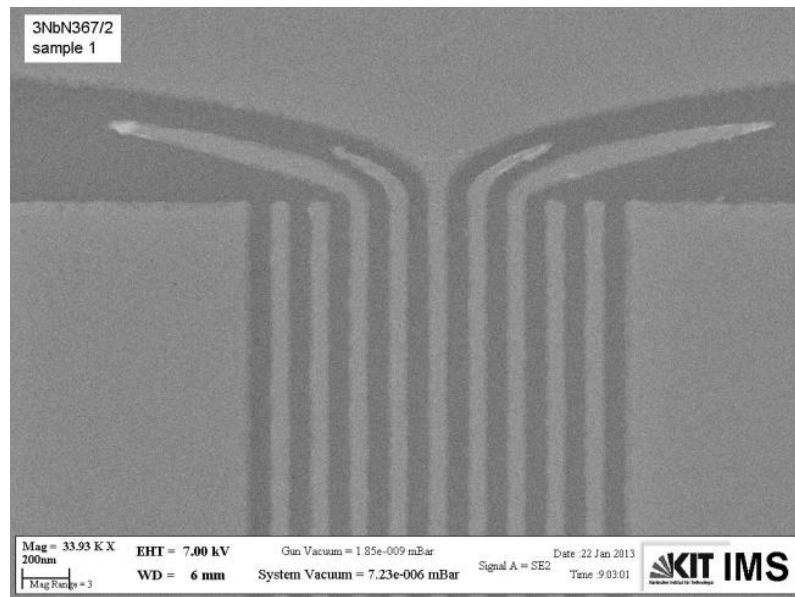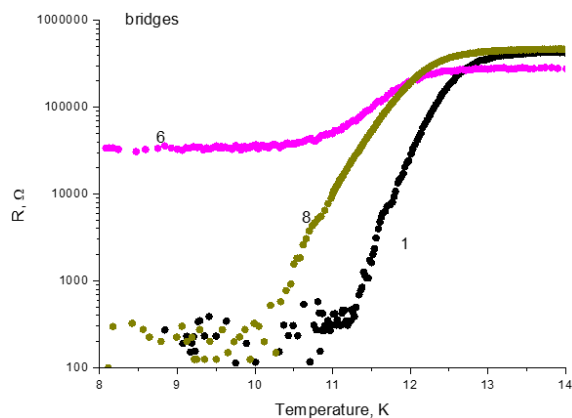
Fig. 21: Critical magnetic flux density vs. critical temperature, measured with a PPMS. The red line is a linear fit to extrapolate $B_c(0)$.
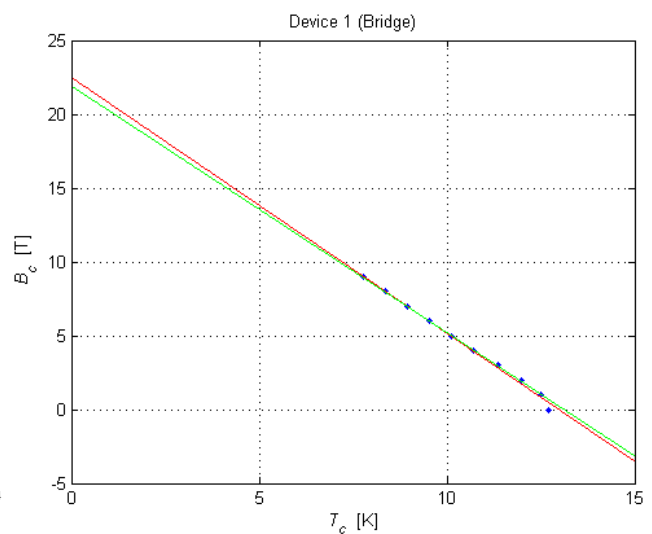
3.1.1 Device preparation

The devices were manufactured by the *Institute for Micro- and Nanoelectronic Systems* of the *Karlsruhe Institute of Technology*. The thin NbN-films were fabricated by direct current magnetron sputtering on substrates of R-plane cut sapphire [23]. The films were then formed into their shape by reactive ion-etching after electron-beam- and photo-lithography (more details in [12]). The outcome were small square plates with edge lengths of a few millimetres carrying the superconducting structures. Those SNSPD-chips were then attached to a sample holder made of copper (only one at a time), where they were connected to a printed circuit board by wire bonding (see section 3.4).

3.2 Cooling

To reach the superconducting state of our detectors, they have to be cooled down below $\approx$ 11-12 K (see Fig. 14, 17, 20). Therefore they are placed in a vacuum chamber inside a ^{3}He- cryostat of Janis Research Company (Fig. 22), where even temperatures < 1 K can be reached. The cryostat consists of an large inner vessel filled with liquid helium (^{4}He, $\sim$ 4 K) and, separated by vacuum, an outer vessel filled with liquid nitrogen ($\sim$ 77 K). A rotary vane pump and a turbopump produce the vacuum. When the cryostat is filled with liquid helium, the vacuum reaches around 10^{-8} mbar.

The temperature of the detector is adjusted manually with a needle valve that regulates the flow of the liquid helium into the 1 K-pot (Fig. 22). Temperatures below 4 K can be achieved by causing the helium to evaporate due to the reduced pressure generated by a rotary vane pump and thus to cool the pot because of latent heat.

Very low temperatures can be achieved using the interaction of charcoal (its temperature is controlled by a heater or helium gas) and the ^{3}He in a container mounted on the top of the cryostat. Condensed ^{3}He drips through a steel tube that is thermally connected to the 1-K-pot into the ^{3}He-pot placed right above the sample holder where the detector is attached. By letting the ^{3}He evaporate in the ^{3}He-pot, detector temperatures as low as 0.5 K can be reached. For more details see [24].

In our experiments, we measured at three different temperatures: 6 K, 4 K and 2 K. Those temperatures could be stabilized up to $\sim$10 hours.

Inside the cryostat, several sensors were placed to monitor the temperatures and the filling level of the liquid helium, which had to be refilled on every day of measuring. The liquid nitrogen vessel had to be filled about once per week.
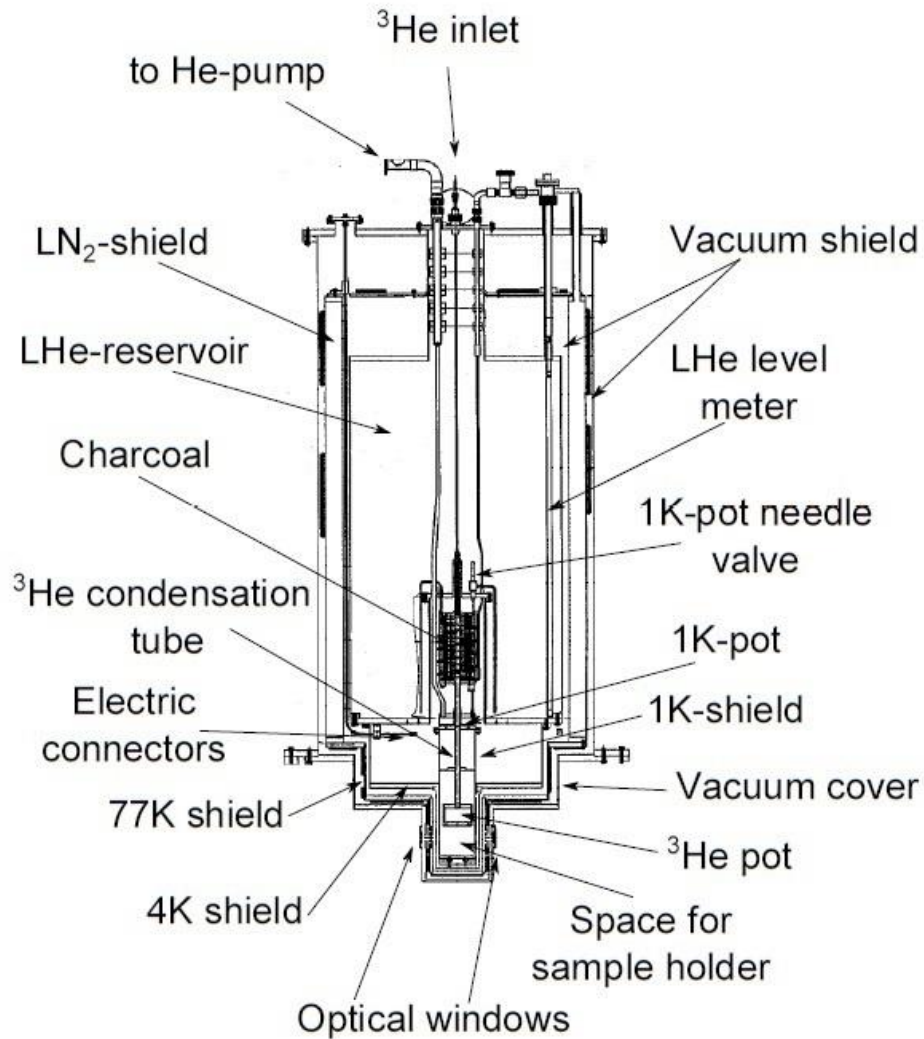
Fig. 22 a), [24]*:* Sketch of ^{3}He-Cryostat used to cool the SNSPDs down to 2 K, 4 K and 6 K.

Fig. 22 b):
Photograph of the part of the cryostat where the detector on the sample holder is placed beneath the ^{3}He-pot.

See also Fig. 23.
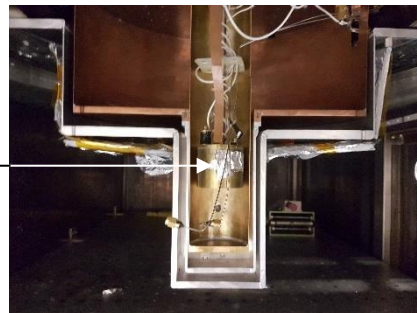
3.3 Magnetic field

The magnetic field the detector is to be exposed to is generated by a mobile electromagnet with iron core placed outside of the cryostat as close to the detector as possible. A Hall effect sensor is placed in close proximity to the detector to measure the magnetic flux density perpendicular to the meander plane. The voltage applied to the electromagnet is provided by a Keithley Source Meter that is controlled by a LabVIEW-software developed by A. Engel. The current through the electromagnet's coil is varied between 0 and $\pm$ 1.2 A, generating magnetic flux densities up to around $\pm$10 mT at the detector's location.

3.4 Electronics

Fig. 23 shows the electronics in the immediate vicinity of the SNSPD-chip, including a Cernox thermo-meter. The SNSPD is connected to a circuit that leads a voltage pulse arising in its superconducting wire over an SMA connector to a mini coaxial cable ('detector signal port'). In Fig. 24 the complete electronic set-up is shown. The voltage signal of the SNSPD is amplified twice, once inside the cryostat and once outside at room temperature, where the signal is lead through another coaxial cable, passes two

Fig. 23, [12]: Image of the electronics on the sample holder, where the SNSPD ('clamped detector') is placed.

attenuators (to damp potential reflections) and then reaches an oscilloscope. The oscilloscope is programmed to record any voltage signals exceeding a certain threshold including the corresponding time information.

The voltage to induce the bias current through the SNSPD's wire is supplied by a Keithley Source Meter 2410 and is brought to the detector with a coaxial cable. Two low-pass filters are used to reduce electronic noise.

Both the Keithley Source Meter generating the bias current and the oscilloscope itself are controlled by a computer using a LabVIEW software of A. Engel, where the settings of a measurement series can be specified.

Fig. 24, slightly adapted from [12]: Electronic setup to measure the voltage pulses generated by the SNSPD with an oscilloscope.

3.5   Measurements

3.5.1   Current-voltage-characteristics

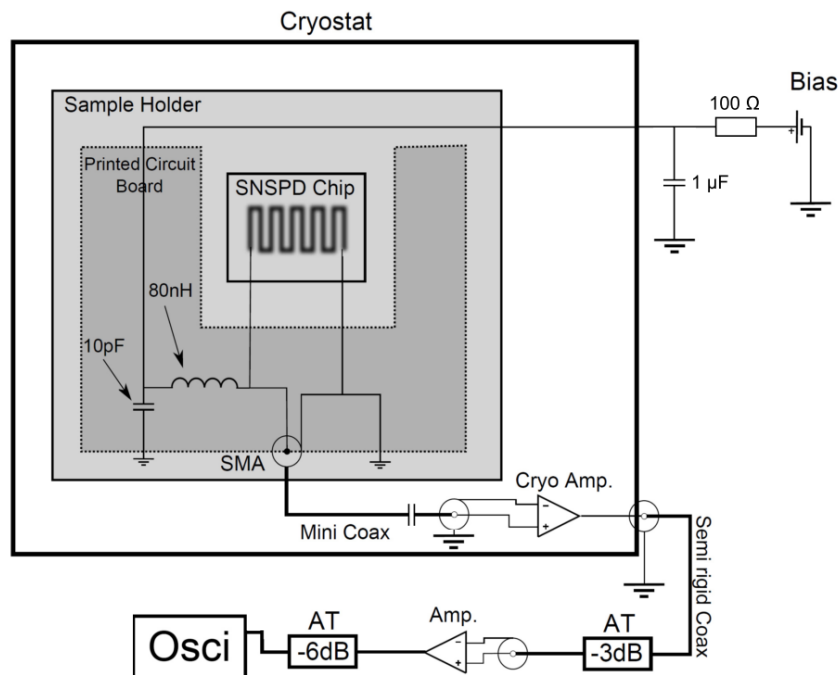To determine the critical current of the detectors at different temperatures and magnetic fields, the current-voltage-characteristics are measured as follows. With measurements of the detector-currents induced by different applied voltages, the scale of the voltage causing the superconducting nanowire to transform into the normal state can be determined. More precise measurements where the voltage in the critical range is altered by 0.05 mV are then executed. The voltage is increased from zero to a value certainly above the critical value and decreased back to zero, both for positive and negative sign. The induced currents are measured and saved in a file. All of this, including the Keithley Source Meter supplying the voltage and the one measuring the current, is operated and read out over a LabVIEW-program prepared by A. Engel.

Each single measurement is repeated fifty times in a row with unaltered settings. The same measurements are then repeated for different magnetic fields (from 0 to $\approx \pm 10$ mT) and again at different temperatures (6 K, 4 K and 2 K).

3.5.2   Dark count rate

The dark count rate is measured by counting the events of the voltage of the detector circuit being lifted over a certain threshold by becoming normally conductive. The oscilloscope saves all voltage signals surpassing the set trigger level until 10'000 such events are counted or a defined amount of time (30 seconds) has passed.

Every time the detector becomes normally conductive a time stamp of the event is recorded by the oscilloscope. The count rate is then calculated as the number of events divided through the time duration from first to last event.

To determine the dark count rate's dependence on the bias current and the magnetic field perpendicular to the detector's plane, the dark count rate is measured for a set of bias currents repeatedly at various coil currents. The bias currents I_b are chosen close to the critical current of the detector at zero magnetic field, I_{c0}.

Each measurement at a certain bias current and coil current is repeated a number of times and the mean of the count rate is saved in an output file that contains a table of information (bias current, number of measurements, temperature, magnetic flux density, resistance, count rate, measurement errors, e.g.). The number of single measurements cannot be chosen too high for a set of measurements, because its overall duration is limited by the liquid helium that does not last longer than approximately 10 hours. It is favourable to measure a whole set at one go and without hours-long pauses, because we found that a measurement with the same settings as a previous one, but performed some days later, could produce results with a small offset to the former ones. The number of measurements was usually set to $n = 10$ or $n = 7$.

To ensure that a magnetic field parallel to the detector plane, respectively parallel to the current running through the detector's nanowire, would not create an effect on the dark count rate, a few measurements are performed with the electro-magnet placed sideways (see Fig. 25) .
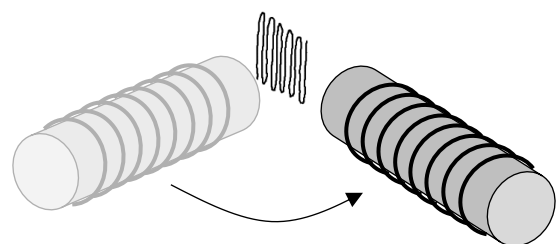

Fig. 25: Sketch of the electromagnet's orientation in regard to the SNSPD.

4 Evaluation and Results

4.1 Current-voltage-characteristics

For each detector we measured the current-voltage-characteristics at three different temperatures $T_1 = 6\,\text{K}, T_2 = 4\,\text{K}$ and $T_3 = 2\,\text{K}$. The applied voltage was increased from zero to an either positive or negative value, so that the corresponding current in the detector-circuit would first increase with the voltage and then drop down as the detector was transitioned into its normal resistive/conducting state. The voltage was then decreased to zero again. This was repeated for various magnetic fields applied perpendicular to the detector plane, with magnetic flux densities $B = \mu_0 H$ up to $\pm 10\,\text{mT}$. In Fig. 26-28 the results for the measurements with no applied magnetic field are shown. Each measurement was run fifty times.
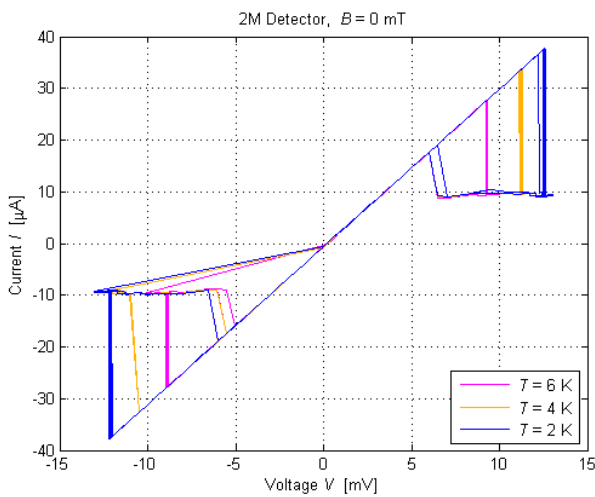

Fig. 26: I-V-characteristics of the meander-SNSPD measured at different temperatures and zero field.
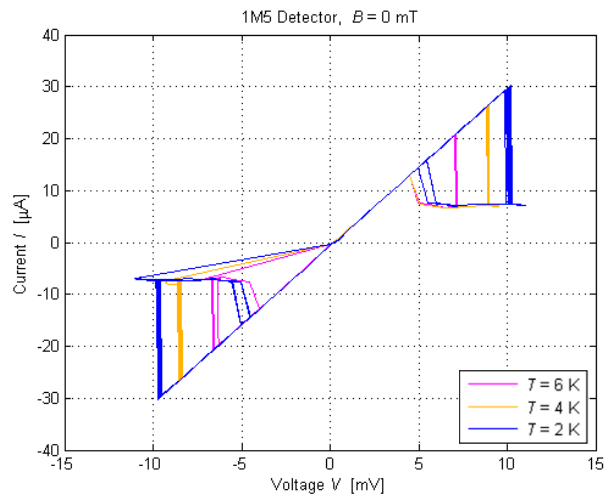

Fig. 27: I-V-characteristics of the 5-turns-meander-SNSPD measured at different temperatures and zero field.
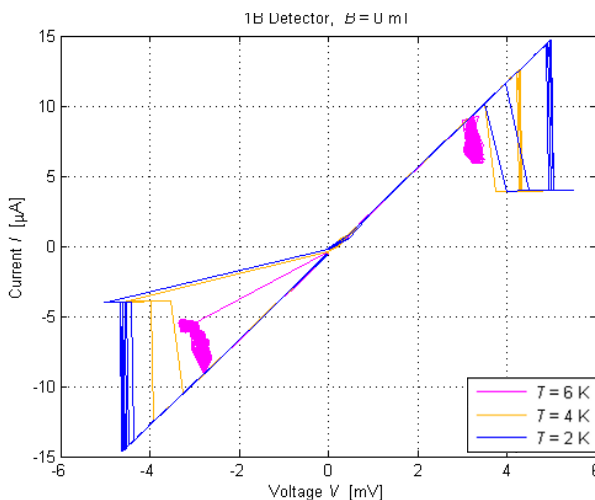

Fig. 28: I-V-characteristics of the bridge-SNSPD measured at different temperatures and zero field.

4.2 Dependence of the critical current on the applied magnetic field

Fig. 29-34 show each detector's determined critical currents I_c depending on the applied magnetic field. The critical currents were identified by finding the highest absolute value reached by the current in each run and then determining the mean value. The error bars show the error of the mean calculated with $\Delta \bar{x} = \frac{s}{\sqrt{n}}$, where s is the standard deviation and $n = 50$ the number of measurements.

In the same plots the theoretical critical current dependence on the magnetic field according to Eq. (1) is shown. The red lines show $I_c(B)$ using the calculated value for $B^* = \mu_0 H^*$ (Eq. (2)), whereas the green lines show $I_c(B)$ calculated with the B^* yielded by fitting the dark count rate data (see section 4.3).

The determined critical currents at zero field for the different detectors, temperatures and current directions are shown in Table 2: *Experimentally determined positive and negative critical currents at zero field for the three different SNSPDs and at different temperatures.*Table 2.

	Critical Current $I_c(0)$ in µA					
	Meander 2M		5-Meander 1M5		Bridge 1B	
T	$I_b > 0$	$I_b < 0$	$I_b > 0$	$I_b < 0$	$I_b > 0$	$I_b < 0$
6 K	27.59 (± 0.01)	−27.59 (± 0.01)	20.71 (± 0.01)	−20.56 (± 0.02)	9.17 (± 0.07)	−9.17 (± 0.02)
4 K	33.47[4] (± 0.04)	−33.27 (± 0.01)	26.31 (± 0.01)	−26.41 (± 0.02)	12.54 (± 0.005)	−12.490 (± 0.001)
2 K	37.49 (± 0.06)	−37.49 (± 0.04)	29.79 (± 0.03)	−29.85 (± 0.03)	14.53 (± 0.02)	−14.49 (± 0.03)

Table 2: Experimentally determined positive and negative critical currents at zero field for the three different SNSPDs and at different temperatures.

4.2.1 Standard meander detector

Fig. 29: Experimentally determined positive (left) and negative (right) critical currents against magnetic field at 6 K; standard meander SNSPD. The red line is the theoretical $I_c(H)$ (Eq. (1)) with the theoretical H^*, the green line is $I_c(H)$ using the H^* determined as output-parameter of the fitting process in section 4.3.
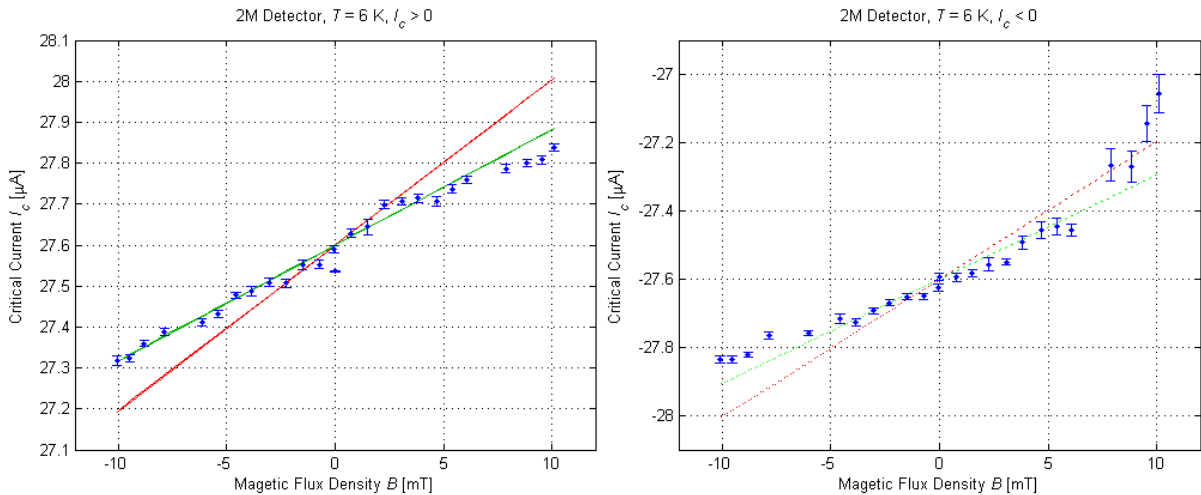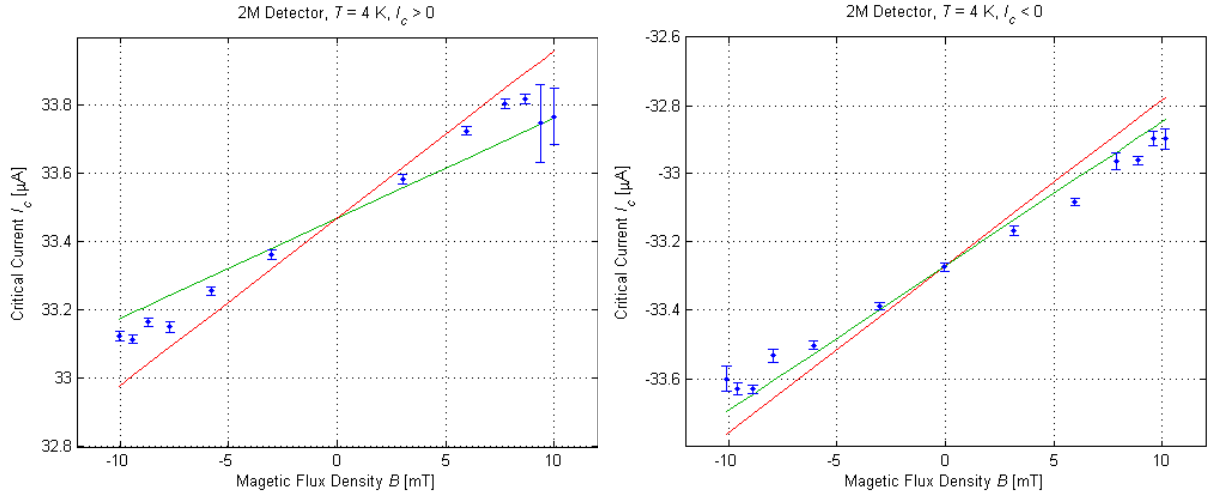
---

[4] Determined by extrapolation

Fig. 30: Experimentally determined positive (left) and negative (right) critical currents against magnetic field at 4 K; standard meander SNSPD. The red line is the theoretical $I_c(H)$ (Eq. (1)) with the theoretical H^*, the green line is $I_c(H)$ using the H^* determined as output-parameter of the fitting process in section 4.3.

4.2.2 Five-turns-detector

Fig. 31: Experimentally determined positive (left) and negative (right) critical currents against magnetic field at 6 K; 5-turns meander SNSPD. The red line is the theoretical $I_c(H)$ (Eq. (1)) with the theoretical H^*, the green line is $I_c(H)$ using the H^* determined as output-parameter of the fitting process in section 4.3.
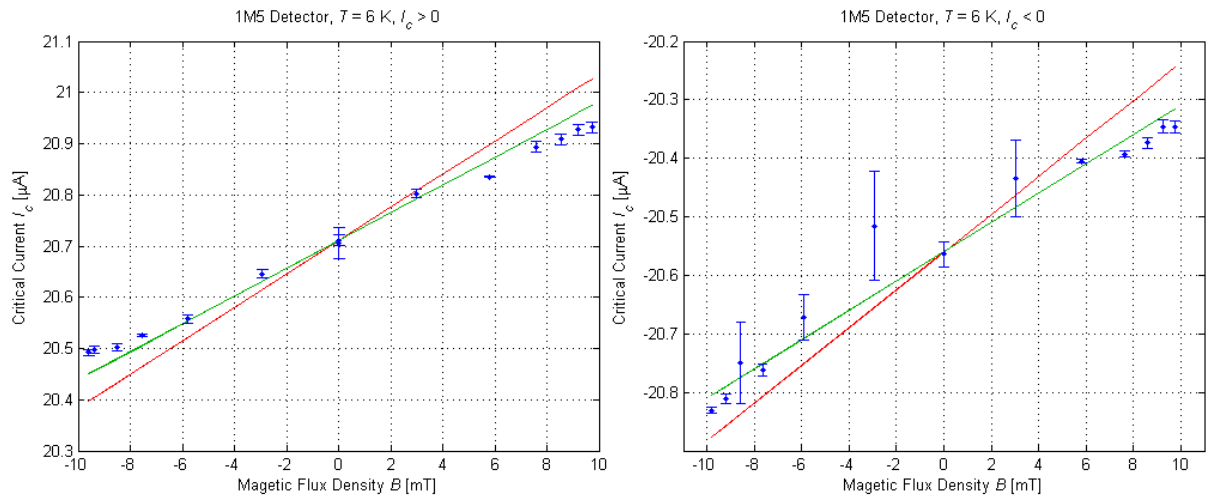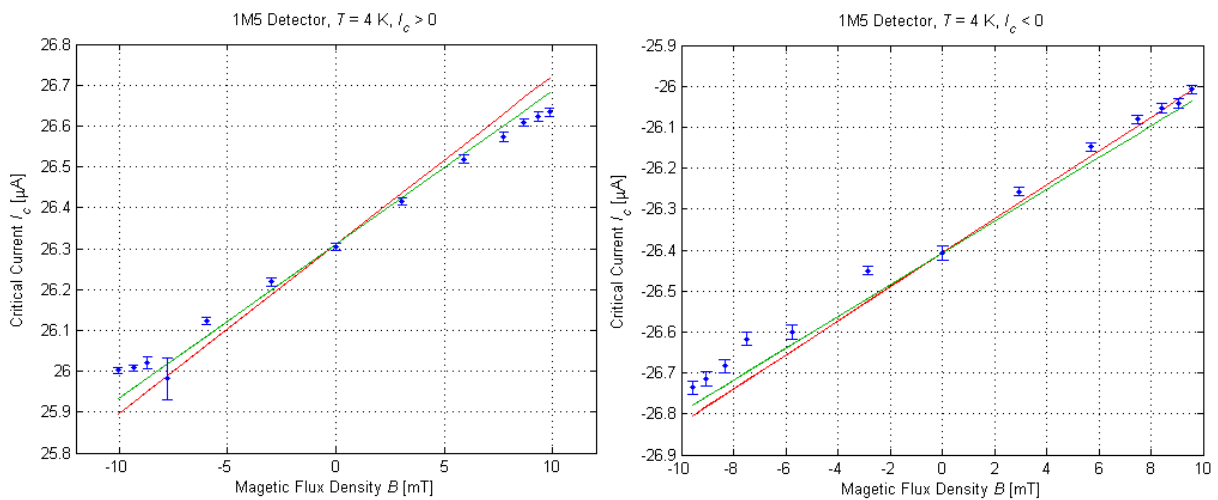

Fig. 32: Experimentally determined positive (left) and negative (right) critical currents against magnetic field at 4 K; 5-turns meander SNSPD. The red line is the theoretical $I_c(H)$ (Eq. (1)) with the theoretical H^*, the green line is $I_c(H)$ using the H^* determined as output-parameter of the fitting process in section 4.3

4.2.3 Single-bridge-detector
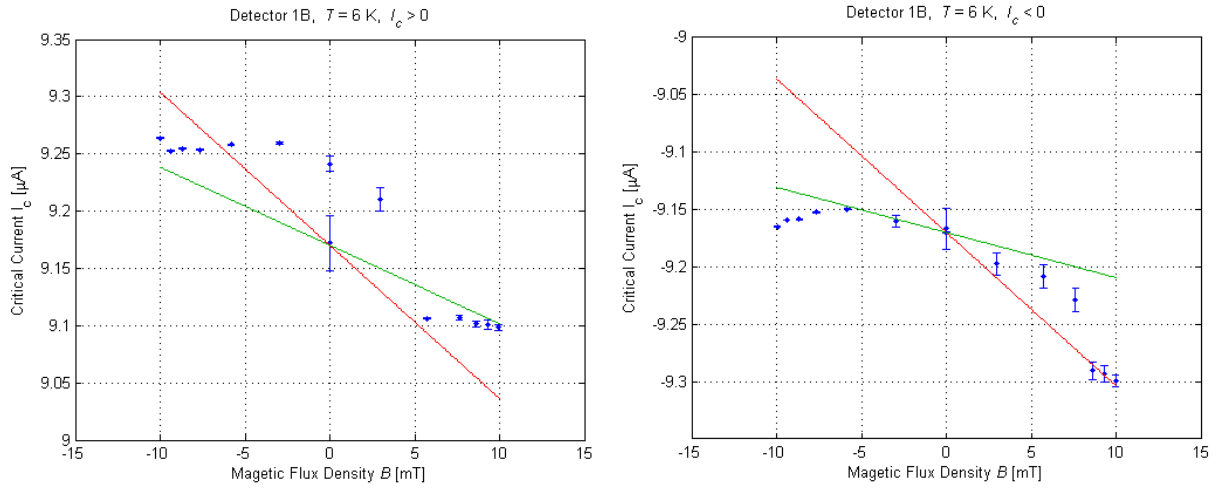
Fig. 33: Experimentally determined positive (left) and negative (right) critical currents against magnetic field at 6 K; single bridge SNSPD. The red line is the theoretical $I_c(H)$ (Eq. (1)) with the theoretical H^*, the green line is $I_c(H)$ using the H^* determined as output-parameter of the fitting process in section 4.3. The data does not match the linear function $I_c(H)$. The positive $I_c(0)$ at 6K was measured twice with different results, as can be seen in the plot on the left.

Fig. 34: Experimentally determined positive (left) and negative (right) critical currents against magnetic field at 4 K; single bridge SNSPD. The red line is the theoretical $I_c(H)$ (Eq. (1)) with the theoretical H^*, the green line is $I_c(H)$ using the H^* determined as output-parameter of the fitting process in section 4.3. The data does not match the linear function $I_c(H)$.
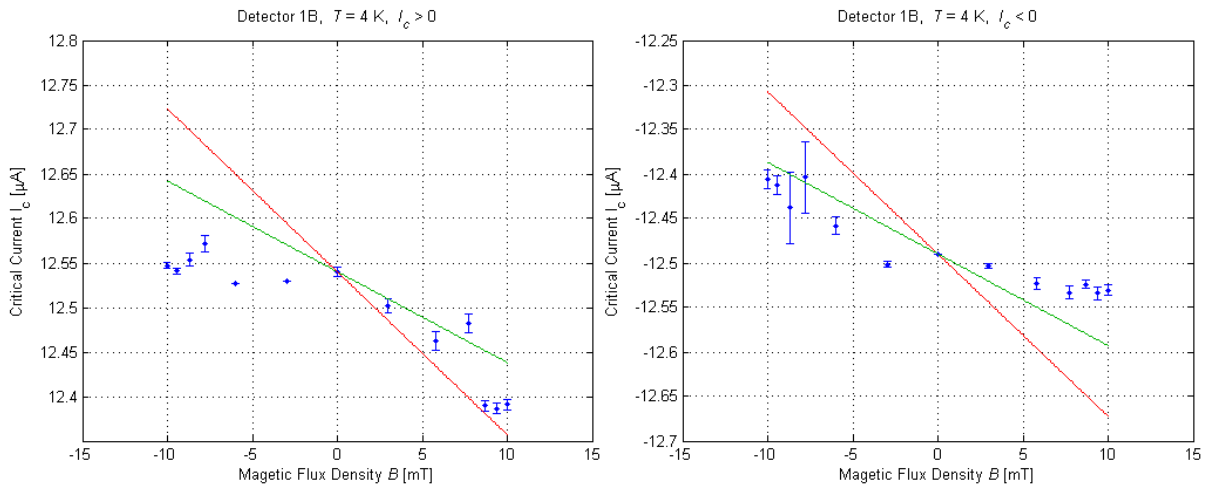
4.3 Dependence of the dark count rate on the applied magnetic field

Each detector's dark count rate determined by the measurements described in section 3.5.2 and slightly modified by the dead time correction (sec. 2.4.1) are plotted against the applied magnetic field in Fig. 35-43. As with Engel's results of similar measurements with a TaN-detector [2], the asymmetry regarding positive and negative magnetic field is apparent.

To find out how good this asymmetry of the dark count rate could be described by the model presented in section 2.4, the data was fitted with the model function (Eq. (7)), but replacing $\frac{H}{H^*}$ with $\frac{B}{B^*} = \frac{\mu_0 H}{\mu_0 H^*}$. The start values of the function's parameters were chosen in the following way.

Meander detectors:

$$R_{DC}^M = R_0 \cdot \left((N-1) \cdot \exp\left(\frac{I_b}{\gamma I_{c0} \cdot \left(1 - \frac{B}{B^*}\right)} \right) + \exp\left(\frac{I_b}{\beta \cdot \gamma I_{c0} \cdot \left(1 - \frac{B}{B^*}\right)} \right) + N \ldots \right.$$
$$\left. \cdot \exp\left(\frac{I_b}{\gamma I_{c0} \cdot \left(1 + \frac{B}{B^*}\right)} \right) \right) \tag{11}$$

Bridge detector:

$$R_{DC}^B = R_0 \cdot \exp\left(\frac{I_b}{\gamma I_{c0} \cdot \left(1 - \frac{B}{B^*}\right)} \right) \tag{12}$$

Fix parameters:

- N is the number of the meander's turns in one direction (e.g. right turns). It is either $N = 14$ for the standard meander detector (2M), or $N = 2$ for the meander with only five turns (1M5).
- The critical current at zero field is determined as described in section 3.5.1.

Fitting parameters:

- The magnetic field scale $B^* = \mu_0 H^*$ was calculated with Eq. (2) in section 2.3.3. The result is used as the start value for the fitting. Depending on the direction of the bias current, it has to have either a positive or a negative sign.

- The start values for γ and R_0 can be found with the formula of the dark count rate in zero field:

$$R_{DC}(H = 0) = R_0 \cdot \exp\left(\frac{I_b}{\gamma \cdot I_{c0}} \right) \tag{13}$$

$$\Rightarrow \ln(R_{DC}) = \ln(R_0) + \frac{I_b}{\gamma \cdot I_{c0}} \tag{14}$$

The natural log function of the dark count rate at zero field is a linear equation with the bias current I_b as the independent variable. Fitting[5] with a straight line yields $\ln(R_0)$ and $\frac{1}{\gamma I_{c0}}$, whereby γ can be identified since I_{c0} is known.

---

[5] Using matlab's polyfit-function

- The start value for "asymmetry-parameter" β was chosen to be $\beta = 0.95$ by trying out what values close to 1 would lead to an adequately shaped graph of the function.

As the values for R_0 are very small (of the order of 10^{-20} to 10^{-70}), the evaluation of the dark count rate data with function (11) or (12) was done by fitting with the natural logarithm of both, thus fitting $\ln(data(I_b, B))$ with $\ln\left(R_{DC}^M(I_b, B)\right) = \ln(R_0) + \ln(\dots)$.

The fitting was done using the least square method in Matlab's surface fitting tool including the data of measurements with a single detector at a single temperature and bias current direction, but for all various bias currents at once. The results are shown in Fig. 35-43. Table 3 lists the parameters' start values and fitted values. Since the formula for R_{DC}^M is extremely sensitive on the parameter γ, it is given with many decimal places.

The data for measurements at $T = 2$ K have not been fitted, because the dark count rates are so low they are not convenient to be evaluated.

	T	I_{bias}	B^* [mT]		γ [1]		β [1]		$\ln(R_0)$ [ln(s^{-1})]	
			start	fit	start	fit	start	fit	start	fit
Standard Meander 2M	6 K	$I_b > 0$	± 682	977.5	0.0082	0.00809	0.95	0.9789	-119.7	-120.1
		$I_b < 0$		-905.7	0.0077	0.00799		0.9797	-122.5	-121.3
	4 K	$I_b > 0$		759.4	0.00557	0.00635		0.9533	-173.8	-160.2
		$I_b < 0$		-786.1	0.0066	0.00704		0.9528	-149.4	-146.1

	T	I_{bias}	B^* [mT]	γ [1]		β [1]		$\ln(R_0)$ [ln(s^{-1})]	
5-turn-Meander 1M5	6 K	$I_b > 0$	± 636	763.1	0.0131 0.0135	0.95	0.9590 -63.7	-62.9 -63.7
		$I_b < 0$		-822.4	0.0121 0.0125		0.9533 -71.0	-69.3 -71.0
	4 K	$I_b > 0$		700.0	0.0095 0.0115		0.8222 -93.1	-92.5 -93.1
		$I_b < 0$		-680.3/ -702.2	0.0094	0.0116/ 0.0124		0.8627/ 0.8043 -87.4/ -88.7	-93.0 -87.4/ -88.7

	T	I_{bias}	B^* [mT]	γ [1]				start	fit
Bridge	6 K	$I_b > 0$	± 685	1340	0.0159	0.01663		-49.8	-47.4
		$I_b < 0$		-2331	0.0073	0.00757		-127.4	-122.7
	4 K	$I_b > 0$		1230	0.0111	0.01083		-79.95	-82.0
		$I_b < 0$		-1213	0.0110	0.01080		-80.69	-82.59

Table 3: Start values to fit the measured data with functions (11) and (12), and the fitting's output values.

The output-values for the scale factor B^* are all larger than the theoretical value, especially for the bridge detector, where it is almost twice as much. Moreover, it is always smaller at the lower temperature. This deviation from the theoretical value (Eq. (2)) could arise from only calculating on the superconducting coherence length at zero temperature, $\xi(0)$, and not $\xi(6\text{ K})$ or $\xi(4\text{ K})$, which would be smaller, thus B^* larger.

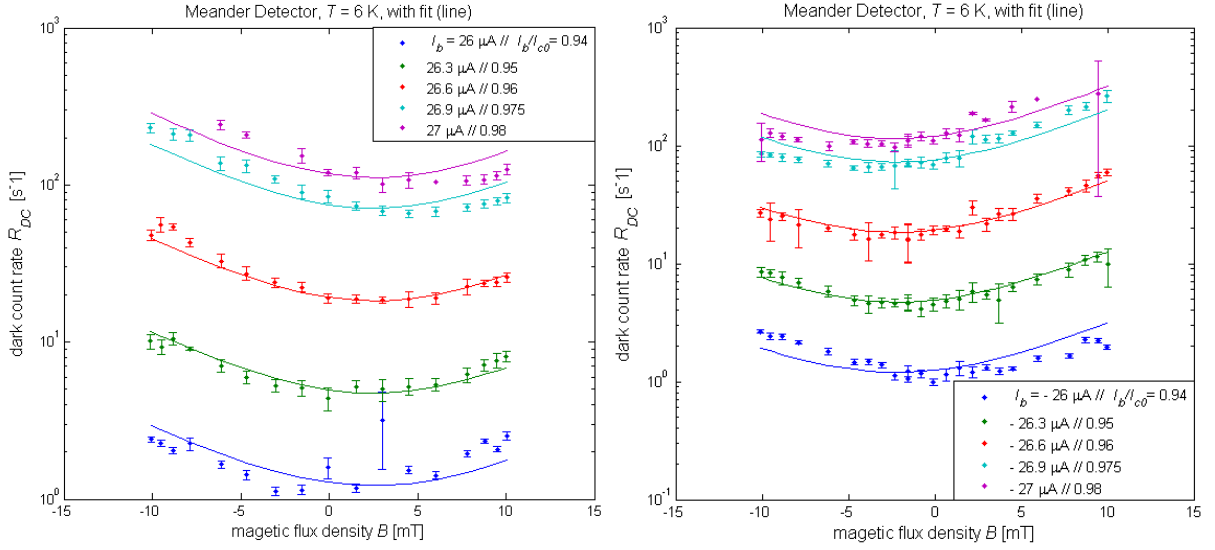### 4.3.1 Standard meander detector (2M)

Fig. 35: Dark count rate against magnetic field at 6 K for positive (left) and negative (right) bias currents. The lines are fits with function Eq. (11).
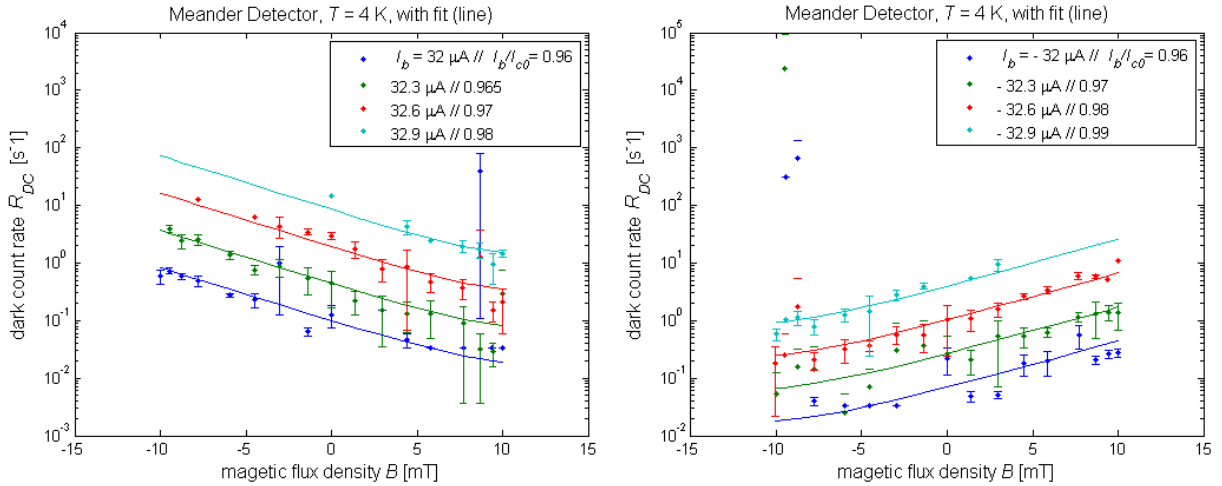

Fig. 36: Dark count rate against magnetic field at 4 K for positive (left) and negative (right) bias currents. The lines are fits with function Eq. (11).

The measured dark count rates of the standard meander detector reach a few hundred counts for bias currents at ≈ 98% of the critical current at 6 K, but are smaller at 4 K by about a factor hundred. At the lower bias currents of ≈ 96-97 %, the count rates at 4 K are so low the deviation from one measurement to another can become relatively high. At both temperatures, a clear asymmetry regarding the sign of the applied magnetic field is apparent. It is even more pronounced at 4 K, where for a magnetic field with the same sign as the bias current, the dark count rate is lower than that at zero magnetic field and the lowest dark count rates are measured for the strongest magnetic field in the corresponding direction.

The effect of the magnetic field seems to be greater at the lower temperature (4 K), where the difference between the lowest and highest dark count rate at a single bias current is around a factor of ten. At a given temperature, the dark count rates are more asymmetric for bias currents closer to the

critical current or at higher count rates, respectively. This cannot be satisfied by our model function, as one can see in the plots.

Fig. 37 shows both the dark count rates for positive and negative bias currents in the same plots, but with the data for negative bias currents (circles) plotted against $-B$ instead of B. It is visible that, at 6 K, reversing both current and field direction leads to practically the same dark count rates. However, at 4 K there is a small offset.

In summary, on the standard meander detector, the effect of the magnetic field is greater at lower temperatures and at higher normalized bias currents I_b/I_c. However, when comparing the results at 6 K with those at 4 K, the extent of the asymmetry is not similar for similar count rates.
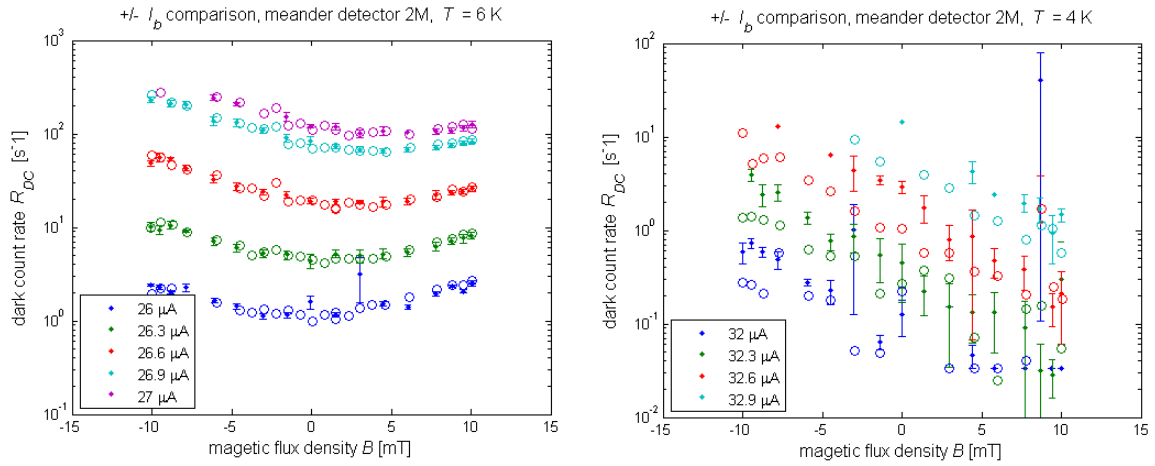

Fig. 37: Comparison of the dark count rates at positive and negative bias currents, (left) at 6 K and (right) at 4 K. The x-axis is reversed for the negative data (circles).
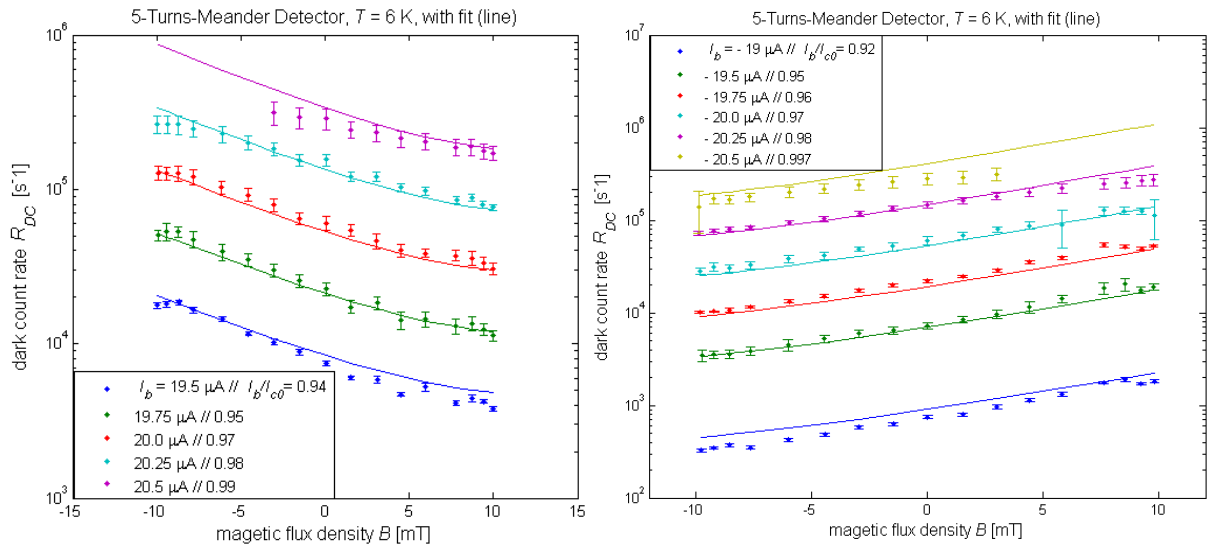
4.3.2   Five-turns meander detector (1M5)

Fig. 38: Dark count rate against magnetic field at 6 K for positive (left) and negative (right) bias currents. The lines are fits with function Eq. (11).
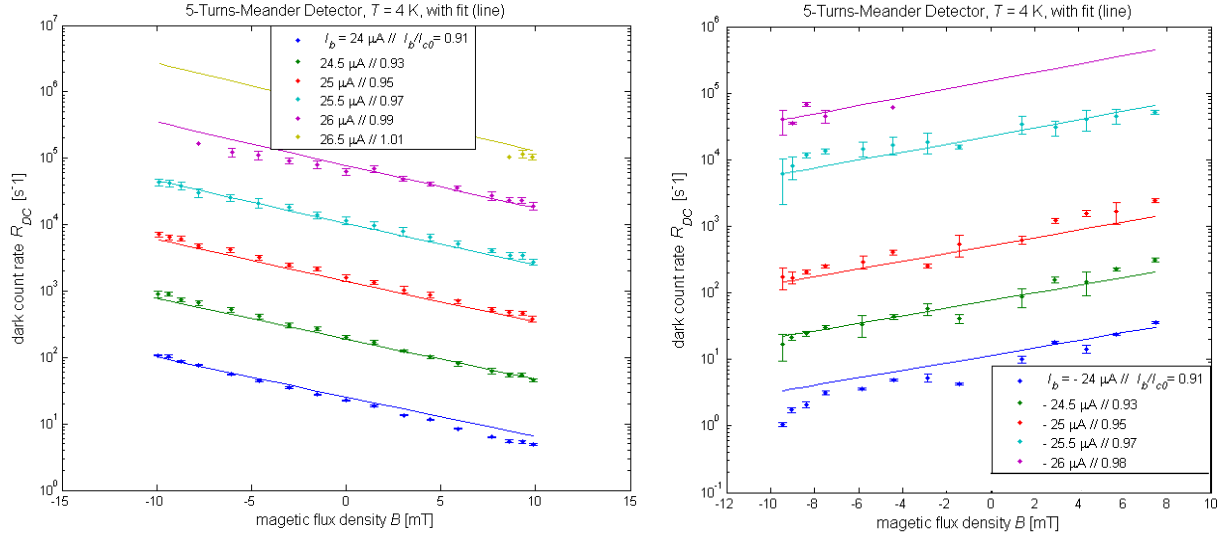
Fig. 39: Dark count rate against magnetic field at 4 K for positive (left) and negative (right) bias currents. The lines are fits with function Eq. (11).

At 4 K, the measurements at a negative bias current have been done twice. In Fig. 40 the results for measurements are shown, where the dark count rate was determined for only two bias currents, but with every measurement repeated twenty-five times instead of the usual ten. The bias current values were chosen on the basis of being close to the critical current, but still allowing stable measurements; meaning that the detector would not be transformed to the normal state and then stay there until the bias current would be turned off[6]. The results for the usual measurements with various bias currents and ten repetitions are shown in Fig. 39 (right). There seems to be something odd about them, since the dark count rates are decreasing a little close to zero field, and the count rates do not quite match those at positive bias currents (see Fig. 41).
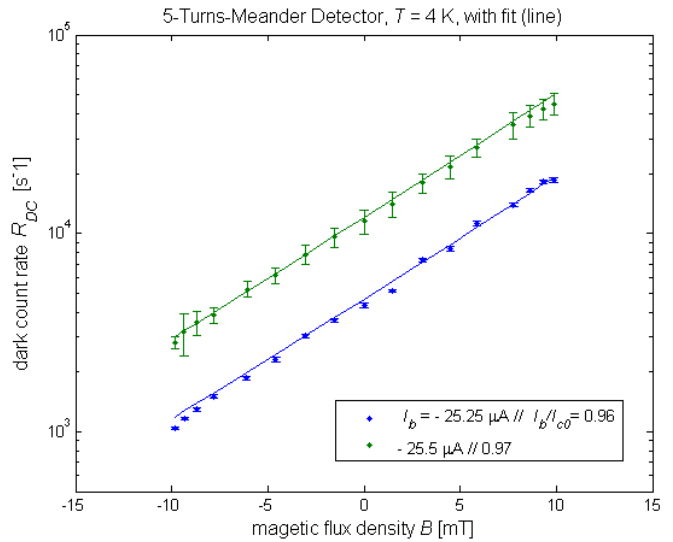

Fig. 40: Dark count rate against magnetic field at 4 K for negative bias currents, mean of 25 measurements. The lines are fits with function Eq. (11).

Overall, the dark count rates of the five-turns-detector show an asymmetry regarding to the magnetic field, too. Assuming that the turns are the dominant areas to cause dark counts, this could be expected, since there is an odd number of turns, therefor one more bend to either the right or left.

What can be surprising, is, that the dark count rate here is by a factor thousand or more higher than that of the standard meander detector with twenty-eight turns, 93.5 % of the strip-width and a total

---

[6] This happened quite often for bias currents very close to the critical current and the magnetic field doing its bit. In Fig. 39 one can see that no data could be measured for the highest bias currents and some fields strengths, because the detector would not relax to the superconducting state.

wire length that is about three and a half times longer. The five-turns-detector does have a critical magnetic field smaller by ca. 90 mT though (see Table 1).
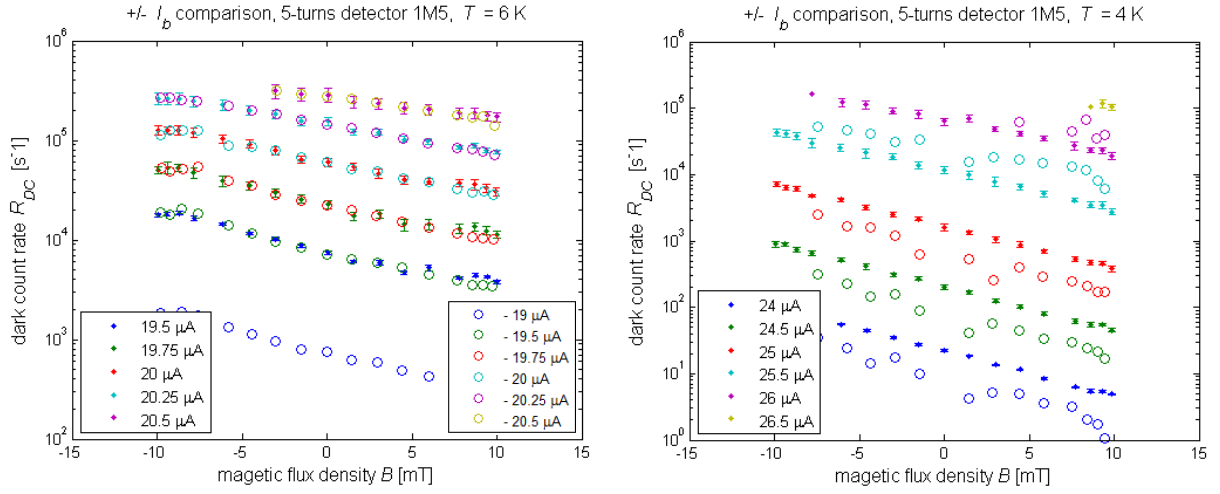

Fig. 41: Comparison of the dark count rates at positive and negative bias currents, (left) at 6 K and (right) at 4 K. The x-axis is reversed for the negative data (circles).

Furthermore, when comparing the dark count rates at different bias currents in one plot, their behaviour appears not to be the same as for the standard meander detector. Here, the ratio $\frac{R_{DC}(-10\text{ mT})}{R_{DC}(+10\text{ mT})}$, that corresponds to the extent of asymmetry, is larger for lower bias currents. Contrary to the 2M-detector results, the dark count rates are not increasing again at higher magnetic fields. If there is a minimum dark count rate at a certain field, it does not lie in-between [-10 mT, 10 mT]. It would be interesting to be able to measure at higher, respectively lower magnetic fields to see if the dark count rate would rise again after decreasing.

Apart from all that, the results of the dark count rates' dependency on the magnetic field are the same here as for the standard meander detector.
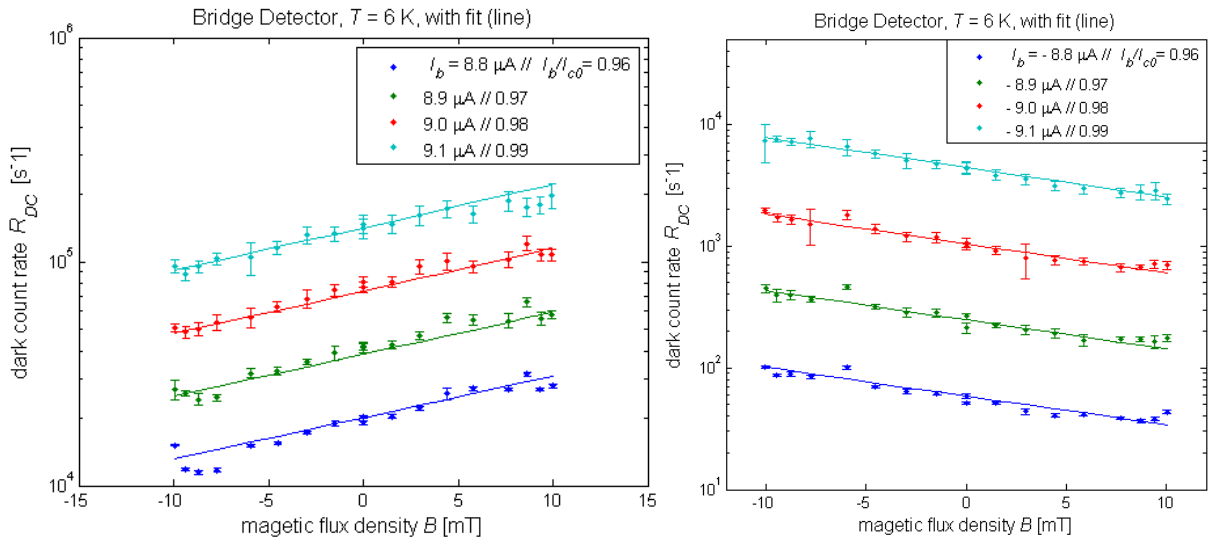
4.3.3 Single bridge detector (1B)

Fig. 42: Dark count rate against magnetic field at 6 K for positive (left) and negative (right) bias currents. The lines are fits with function Eq. (12).
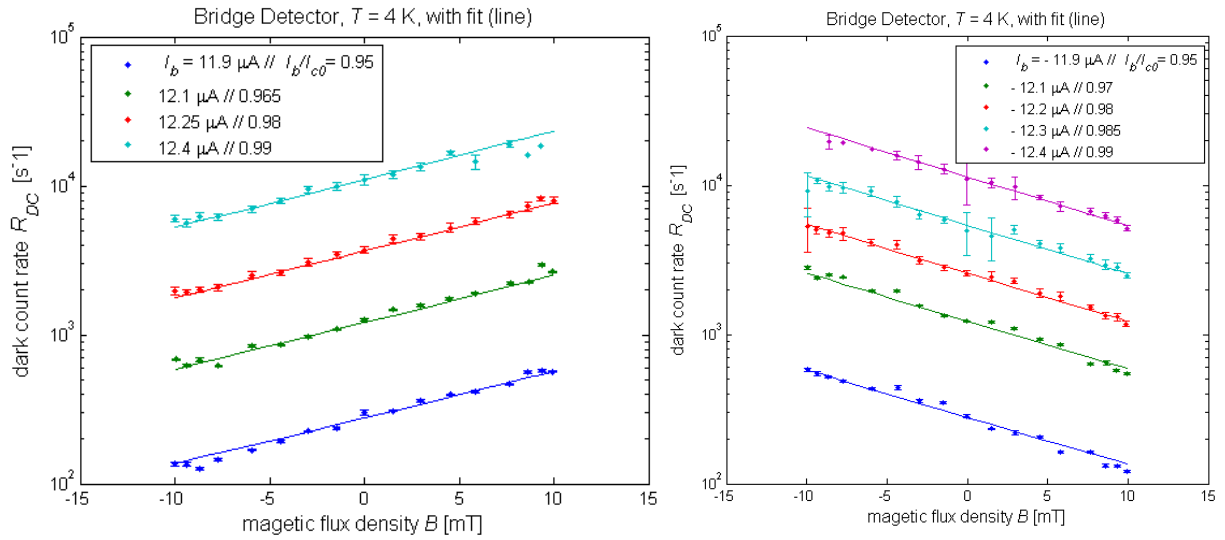
Fig. 43: Dark count rate against magnetic field at 4 K for positive (left) and negative (right) bias currents. The lines are fits with function Eq. (12).

Interestingly, even our single-bridge detector consisting of only a straight strip without any bends does not yield a symmetric dark count rate dependency on the magnetic field, even less than the standard meander detector at 6 K. The determined dark count rates at 6 K are not the same for positive and negative bias currents (see Fig. 44), but at 4 K, they coincide. This could have to do with measuring at 6 K and negative bias currents several days after measuring with the positive bias currents. In contrast, the data at 4 K and negative bias currents was measured the day after measuring with positive bias currents.

A possible explanation for the asymmetry of the dark count rates of the bridge detector could be, analogous to the meander-detectors, that one edge of the straight strip exhibits more imperfections than the other, causing the critical current to decrease when the wire-current is caused to crowd at this edge by the magnetic field, and vice versa.
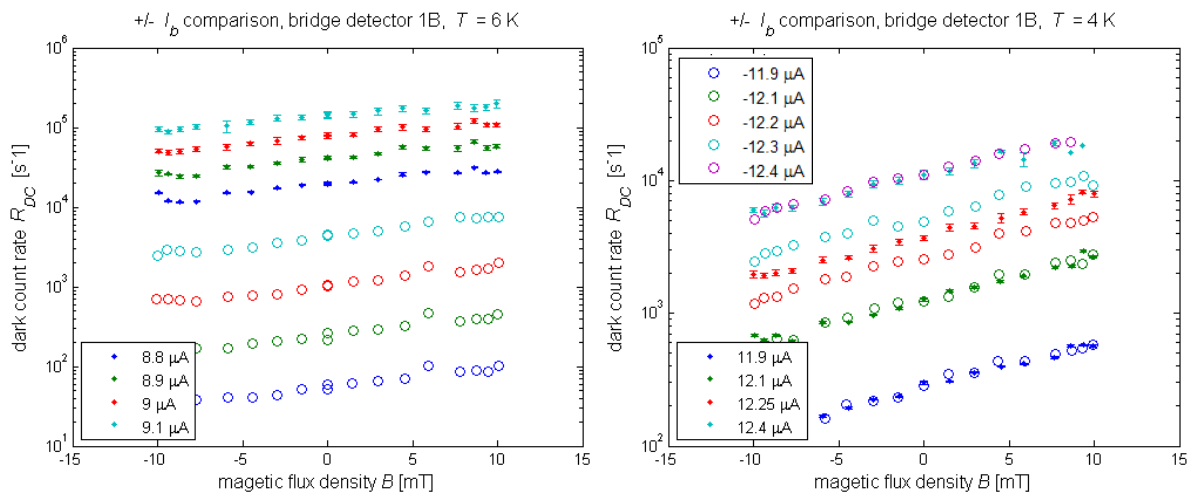

Fig. 44: Comparison of the dark count rates at positive and negative bias currents, (left) at 6 K and (right) at 4 K. The x-axis is reversed for the negative data (circles). The absolute values of the negative bias currents on the left are the same as the positive ones. It is not clear why the count rates are so much higher for positive bias currents.

4.3.4   Effect of dead-time-correction

Fig. 45 shows the effect of the dead-time-correction described in section 2.4.1 by the example of the dark count rates of the 1M5-detector measured at 4 K. As one can see in the diagram, the dead-time-correction with dead time $\tau \approx 2.5$ µs starts to make a difference only at high count rates of about twenty-thousand counts per second. The dead-time-correction could even be greater at those high count rates to fit the model function (fit line) better.
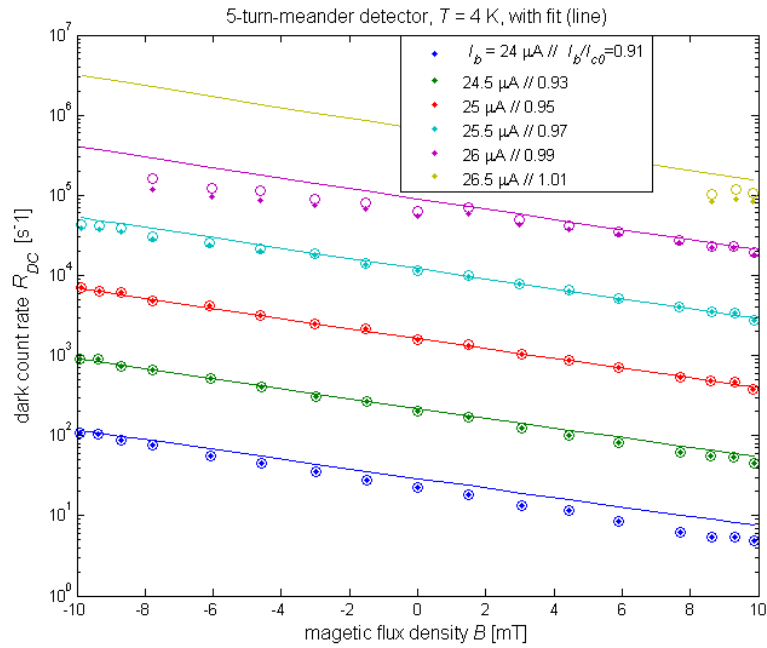

Fig. 45: Dark count rate measured (dots) and after dead-time correction (circles), Eq. (9).

4.3.5 Dependence of the dark count rate on a parallel magnetic field

For the measurements with a magnetic field parallel to the meander-plane of the detectors, the electromagnet was moved accordingly, but the orientation of the Hall sensor was not altered. Therefore, the magnetic flux density parallel to the detector-plane could not be measured, only the perpendicular component. From the other measurements we know what magnetic flux densities certain coil currents produce, though. The maximum current through the electromagnet's coil is set to be $\pm\,1.2$ A, what corresponds with a magnetic flux density of around $10\,\text{mT}$ at the detector's site. So although the x-axis of the following plots shows small, measured values for B, the actual magnetic flux densities the detectors were exposed to vary from $\approx -10\,\text{mT}$ to $\approx 10\,\text{mT}$.

As expected, there is no significant effect of a magnetic field parallel to the detectors' meander-planes (see Fig. 46).
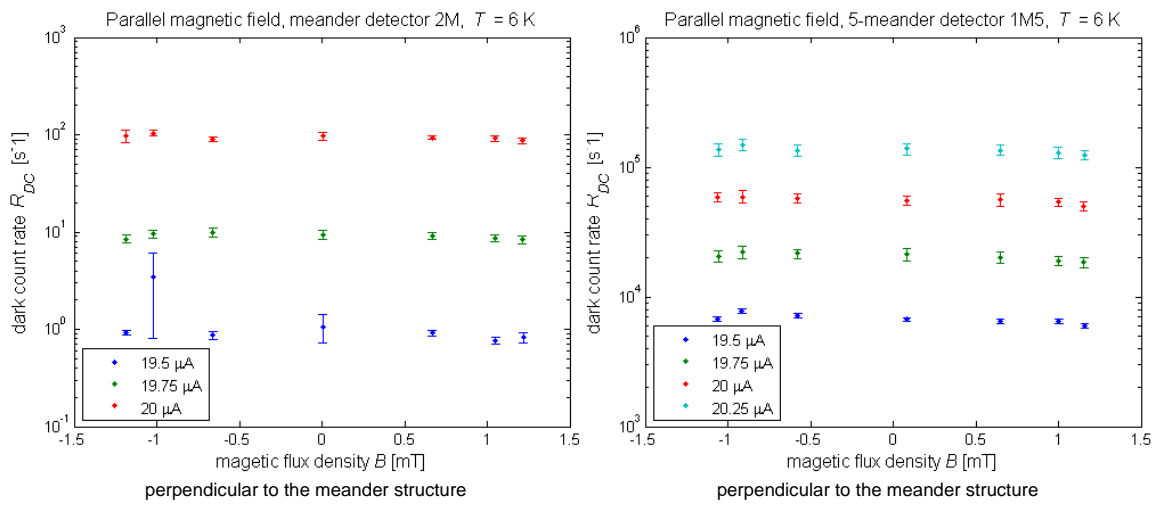

Fig. 46: Dark count rates against a magnetic field from $-10\,mT$ to $10\,mT$ that was placed parallel to the detector plane.

5 Conclusion

The asymmetric dependence of the dark count rate on an perpendicularly applied magnetic field found by [2] could be reproduced with three different NbN-SNSPDs. The model, that focuses on the 180° turns of the detectors' meander-structure and assumes crossing vortices to be the main reason for dark counts was able to describe our measured data well. The factor β, representing the inequality of the meander-turns, respectively their contributions to generating dark counts, could be made conditional on the bias current to yield even better accordance of the model to the data. Even the dark count rates of the detector consisting of only a straight strip without bends showed a distinct asymmetry in regard to the sign of the applied magnetic field. In the meander-shaped detectors, this asymmetry is more pronounced at the lower temperature 4 K than at 6 K. Our measurement results with the lowest asymmetry were those of the standard meander detector at the lowest bias current and 6 K. The greatest effect of the magnetic field on the dark count rate was observed in the five-turns meander detector at 4 K, but interestingly also at the lowest bias current.

Our results suggest, what was already assumed. In addition to narrow bends, imperfections of the strip edges play a part in increasing the dark count rate by causing current crowding and thus lowering the energy barrier for vortices to enter the superconducting strip. Depending on its direction, a perpendicular magnetic field causes the current density to either increase or decrease at a certain edge. That way, also the dark count rate can either be increased or decreased.

In order to manufacture SNSPDs with as low dark count rates as possible, a convenient combination of material-choice, strip-shape, accurate fabrication, operation temperature and bias current could accomplish the purpose. Bulaevskii et al. [17] claim, that an "optimum current exists, which minimizes the effect of dark counts, while only weakly diminishing photon counts". Detectors with strips that bend only in one direction, such as a spiral shape, are also promising, as mentioned by [21]. Such a SNSPD was implemented by J. Huang *et al.* [25] with a dark count rate of 100 Hz. They stated that "no meaningful current crowding effect was observed".

Acknowledgements

References

[1]   R. H. Hadfield, "Single-photon detectors for optical quantum information applications", *Nature Photonics*, vol. 3, p. 696-705, 2009.

[2]   A. Engel, A. Schilling, K. Il'in and M. Siegel, "Dependence of count rate on magnetic field in superconducting thin-film TaN single-photon detectors", *Physical Review B - Condensed Matter and Materials Physics*, vol. 86, p. 1-4, 2012.

[3]   L. N. Cooper, "Bound Electron Pairs in a Degenerate Fermi Gas", *Phys. Rev.,* vol. 104, 1189, 1956.

[4]   V. L. Ginzburg, L. D. Landau: "To the Theory of Superconductivity", *L. D. Landau: Collected papers,* Pergamon Press, Oxford, 1965.

[5]   J. Eck, "Superconductor Information for the Beginner", on superconductors.org/terms.htm, last viewed Oct. 2017.

[6]   L. J. Gauckler (?), "Supraleitung", lecture *Ceramic II*, 2009 at ETH Zurich, retrieved from http://www.nonmet.mat.ethz.ch/education/courses/ceramic2/Kap8_2009.pdf.

[7]   B. Deaver, W. Fairbank, "Experimental Evidence for Quantized Flux in Superconducting Cylinders", *Physical Review Letters*, vol. 7, 1961.

[8]   R. Doll, M. Näbauer, "Experimental Proof of Magnetic Flux Quantization in a Superconducting Ring", *Physical Review Letters*, vol. 7, 1961.

[9]   G. Stan and S. B. Field, "Critical fields for vortex expulsion from narrow superconducting strips", Physical Review B - Condensed Matter and Materials Physics, vol. 75, p. 1-4, 2007.

[10]   L. N. Bulaevskii, M. J. Graf, and C. D. Batista, "Vortex-induced dissipation in narrow current-biased thin-film superconducting strips", *Physical Review B - Condensed Matter and Materials Physics*, vol. 83, p. 1-9, 2011.

[11]   C. Natarajan, M. Tanner, R. Hadfield, "Superconducting nanowire single-photon detectors: physics and applications", *Superconductor Science and Technology*, vol. 25, p. 063001, 2012.

[12]   K. Inderbitzin, "Superconducting Nanowires for Soft X-Ray Single-Photon Detection", Dissertation, University of Zurich, 2013.

[13]   H. Bartolf, "Fabrication and Characterization of Superconducting Nanowire Highspeed Single-Photon Detectors", Dissertation, University of Zurich, 2009.

[14]   H. Shibata H, M. Asahi, T. Maruyama, T. Akazaki, H. Takesue, T. Honjo and Y. Tokura, "Optical response and fabrication of MgB2 nanowire detectors", *IEEE Trans. Appl. Supercond.*, vol. 19, 2009

[15]   A.E. Lita, V.B. Verma, R. D. Horansky, J.M. Shainline, R.P. Mirin and S. Nam, "Materials Development for High Efficiency Superconducting Nanowire Single-Photon Detectors", *MRS Online Proceedings Library (OPL)*, vol. 1807, p. 1-6, 2015.

[16]   Il'in, K. S., M. Lindgren, M. Currie, A. D. Semenov, G. N. Gol'tsman, R. Sobolewski, S. I. Cherednichenko and E. M. Gershenzon, "Picosecond Hot- Electron Energy Relaxation in NbN Superconducting Photodetectors", *Appl. Phys. Lett.,* vol. 76, 2000.

[17] L. N. Bulaevskii, M. J. Graf and V. G. Kogan, "Vortex-assisted photon counts and their magnetic field dependence in single-photon superconducting detectors", *Physical Review B - Condensed Matter and Materials Physics*, vol. 86, p. 1-10, 2012.

[18] R. Lusche, "Einfluss von Geometrie und magnetischem Feld auf die Effizienz supraleitender Nanodraht- Einzelphotonendetektoren", Dissertation, Technische Universität Berlin, 2015.

[19] K. K. Likharev, "Superconducting weak links," *Rev. Mod. Phys.*, vol. 51, p. 101–159, 1979.

[20] J. R. Clem, K. Berggren, "Geometry-dependent critical currents in superconducting nanocircuits", *Physical Review B - Condensed Matter and Materials Physics*, vol. 84, p. 1-27, 2011.

[21] J. R. Clem, Y. Mawatari, G. R. Berdiyorov and F. M. Peeters, "Predicted field-dependent increase of critical currents in asymmetric superconducting nanocircuits", *Physical Review B - Condensed Matter and Materials Physics*, vol. 85, p. 1-16, 2012.

[22] R. Willink, "On dead-time corrections for estimating rates", *Measurement Science and Technology*, vol. 21, 2009.

[23] K. Il'in, M. Siegel, A. Engel, H. Bartolf, A. Schilling, A. Semenov, and H.-W. Hübers, "Current-induced critical state in NbN thin-film structures," *J. Low Temp. Phys.*, vol. 151, p. 585–590, 2008.

[24] A. Aeschbacher, "Superconducting Nanowire Single-Photon Detectors based on TaN Thin Films", Master's thesis, University of Zurich, 2011.

[25] J. Huang, W. J. Zhang, L. X. You, X. Y. Liu, Q. Guo, Y. Wang, L. Zhang, X. Y. Yang, H. Li, Z. Wang and X. M. Xie, "Spiral superconducting nanowire single-photon detector with efficiency over 50% at 1550 nm wavelength", *Superconductor Science and Technology*, vol. 30, 2017.

[26] T. Van Phan, "Collective Behaviors of Vortices in thin slab Superconductor of Type I & II", MIT-Website, http://web.mit.edu/8.334/www/grades/projects/projects14/TrungPhan_8334WP/foundation-5.2.2/I_3.html#, 2014, last viewed Oct. 2017.